NPL Report MATC(A)157

The Effect of Temperature on Microstructure of Lead-free Solder Joints

Thomas Le Toux, Milos Dusek & Christopher Hunt

November 2003

The Effect of Temperature on Microstructure of Lead-free Solder Joints

Thomas Le Toux, Milos Dusek and Christopher Hunt

National Physical Laboratory
Teddington, Middlesex, UK, TW11 0LW

ABSTRACT

Samples of surface mounted components cooled during their solidification process were subjected to aging treatment in accelerated way to develop microstructural changes. Microsections of solder joints were analysed and methods for measurement of characteristic size of Sn-dendrite is proposed. These tools can be used to detect structures (such as dendrites, dendrites grains, or intermetallic features).

The impact of cooling rate and iso-thermal ageing on the microstructure of lead-free alloys as used in surface mount joints is investigated. The changes in the tin dendrites and intermetallics are measured using image analysis tools developed here. The algorithm developed produces a numerated classification that can be correlated with the aging of the microstructure.

ISSN 1473 2734

National Physical Laboratory
Teddington, Middlesex, UK, TW11 0LW

Approved on behalf of Managing Director, NPL, by Dr C Lea,
Head, Materials Centre

Contents

1.1. Introduction

Mechanical testing of lead-free solders has been under extensive research over last 5 years. The industry currently has the benefit if more than 40 years of reliability data with standard SnPb alloy. As the industry moves forward there is an urgent need to acquire the equivalent data for the lead-free alloy of choice over a compressed time scale. Major reasons for concerns in using lead-free solders are lack of reliability and processability for lead-free alloys. Alloy reliability will be very much a function of the microstructure, which in turns affects properties such as strength, creep, stress relaxation and so on. Clearly only relationship that can be established between microstructure and mechanical properties would be very valuable. However characterising microstructure is complex, a significant issue being the analysis is run on a 2D image, where in actuality the analysis is of the 3D structure. The approach here is to use features occurring in the microsections, measure these and attempt to correlate these with mechanical properties. Further more in this report the effect of cooling rate and temperature conditioning on the microstructure of lead-free solder joints has been investigated.

Tin-silver based solder alloys are leading candidates for lead-free solders in electronic manufacturing. The mechanical performance of a surface mount solder joint depends on its microstructure and this has to be assessed, as a function of processing and storage conditions. Microstructure can be captured by taking cross-sectional images of solder joints, and then processed by image analysers to obtain summarised information about the complex microstructure.

1.2. Description of test specimens

Table 1 lists of sample of aging conditions and includes various aging temperatures and times along with various cooling rates from the molten solder state. The examples of microsectioend specimens are shown in Figure 1 for BGA, SOIC and chip resistor joints. There are two lead-free solders used in the experiment Sn3.5Ag and Sn3.5Ag0.7Cu.

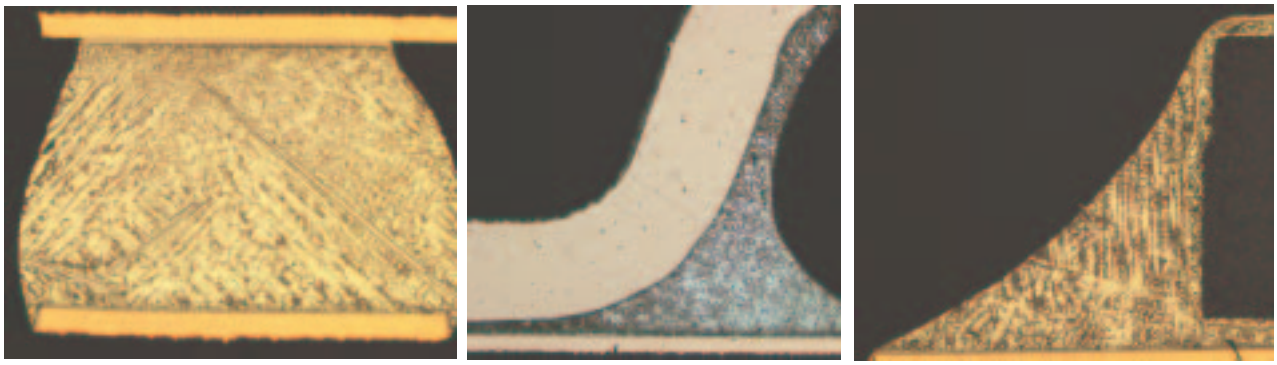

BGA SOIC 0805 chip resistor

Figure 1: Examples of optical micrographs

Table 1 Thermal conditions of the specimens

Designation	Alloy	Aging		Cooling rate
		Temperature [°C]	Time [hours]	[°C/s]
m429	SnAgCu	20	0	0.5
m450	SnAg	20	0	0.5
m428	SnAgCu	20	0	1
m449	SnAg	20	0	1
m427	SnAgCu	20	0	2
m448	SnAg	20	0	2
m426	SnAgCu	20	400	0.5
m425	SnAgCu	20	400	1
m424	SnAgCu	20	400	2
m414	SnAgCu	50	400	0.5
m413	SnAgCu	50	400	0.5
m439	SnAg	50	400	2
m420	SnAgCu	125	400	0.5
m415	SnAgCu	125	400	2
m416	SnAgCu	125	400	2
m412	SnAgCu	50	1000	0.5
m47	SnAgCu	50	1000	2
m45	SnAgCu	125	1000	0.5
m46	SnAgCu	125	1000	0.5
m44	SnAgCu	125	1000	1
m431	SnAg	125	1000	1

Analysis of micrographs involves, identification of common structures such as intermetallics and tin dendrites. The typical microstructure of samples is identified in Figure 2.

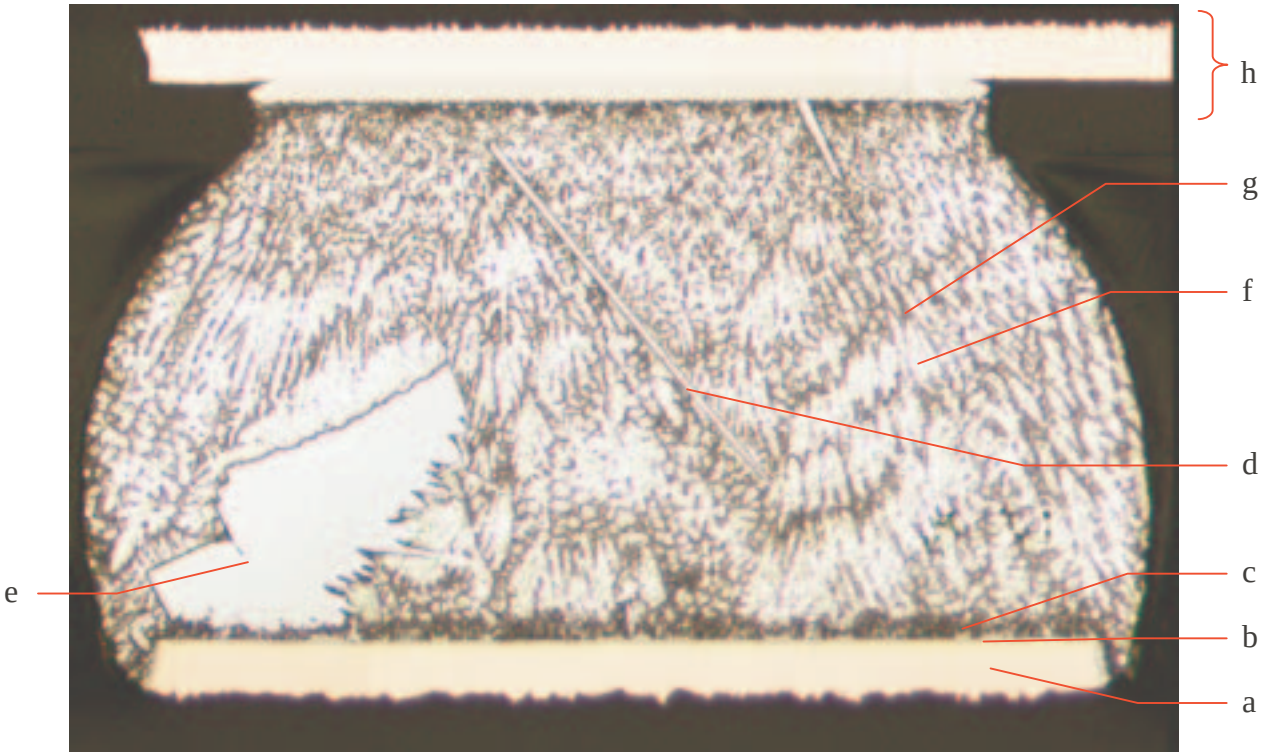

Figure 2: M449BGA7 tin-silver sample

a PCB interconnection. This is a copper layer pad with thickness of 35 µm
b 0.5 µm thin Nickel layer
c Cu_6Sn_5 and Cu_3Sn intermetallic layer with Ni, forming thin “needles” (not clear at this scale)
d Ag_3Sn “flake”
e Ag_3Sn structure oriented perpendicular to structure (d) in lateral plane
f tin dendrites (white)
g matrix of Sn, with Ag_3Sn lamellae (black)
h component interconnection: Cu layer with a Ni barrier (solder mask defined)

As seen in Figure 2 the flake (e) is oriented parallel to microstructural plain which in fact is the same structure as (d).

1.2.1. Examination of dendrites

Sn dendrites are the main visual structures, which can be identified in micrographs from either optical of SEM images. We can observe on micrographs that dendrites are often gathered within colonies shown schematically in Figure 3. The dendrite stems within any one colony are all crystallo-graphically related to a common nucleus.

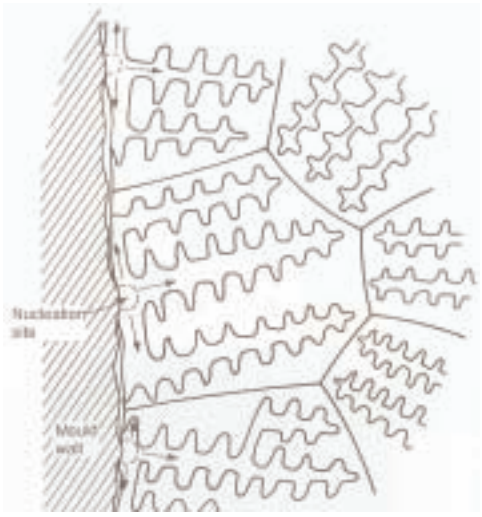

Figure 3: Dendrites grains. The mould wall relates to components interconnections

Figure 4 illustrates typical tin dendrite formation; the figure also reveals a trapped void inside the joint, caused by entrapped gases solidified in the solder joint.

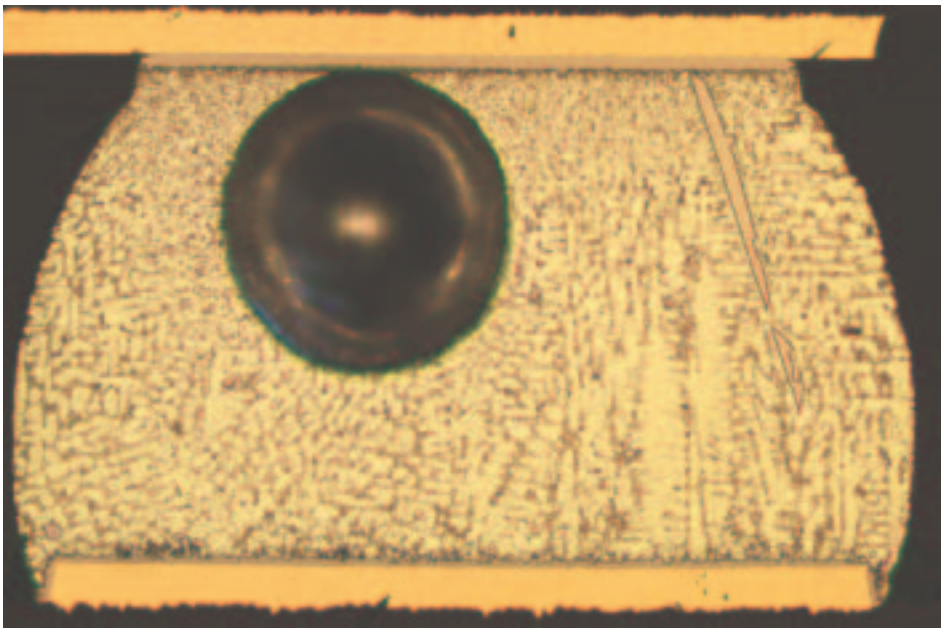

Figure 4: dendrites on M429BGA5

Since a dendrite is a three-dimensional object its appearance on a 2D photograph depends upon the plane of the section.

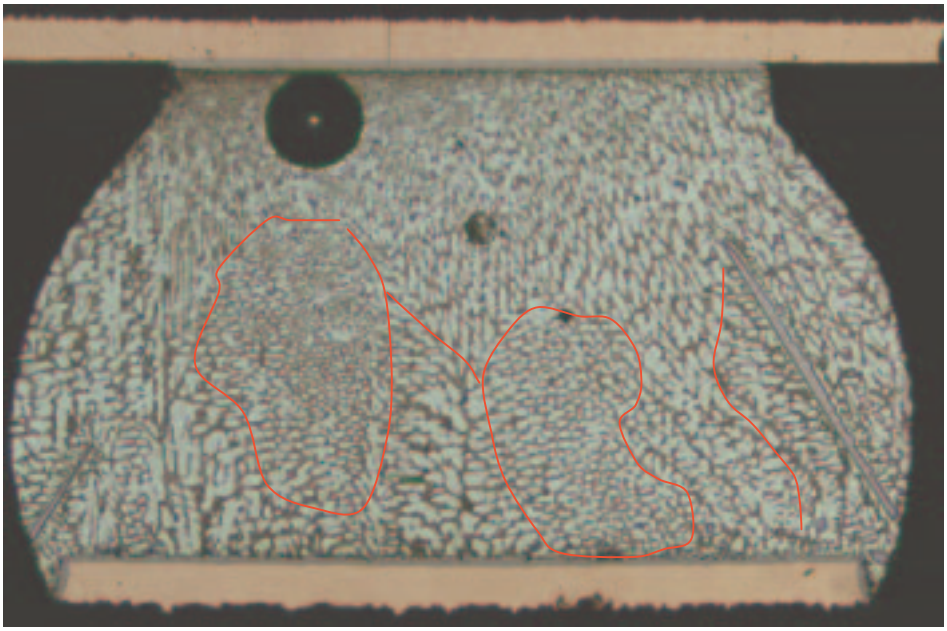

Figure 5: colonies of dendrites, M429BGA5

Analyses have been performed on several samples with a Scanning Electron Microscope (SEM), to confirm the elemental constitution of each structure in the micrographs. While the data is consistent with the expected result the analysed depth, typically few µm may lead to some small errors, and is not thought to be an issue in the following work.

1.2.2. Intermetallic layer along interfaces

These joints show a typical intermetallic layer forming at the interface. The intermetallic layer thickness increases with time and temperature [1]. The starting point of the analysis is to crop images from the various specimens to be evaluated, and converting the images into a 256 grey scale format. Images in this format have better clarity, and are less sensitive to brightness & contrast settings when using colour images. The resulting image is shown in Figure 7a. The transform into a binary image was based on a grey-level histogram (Figure 7b) of the image.

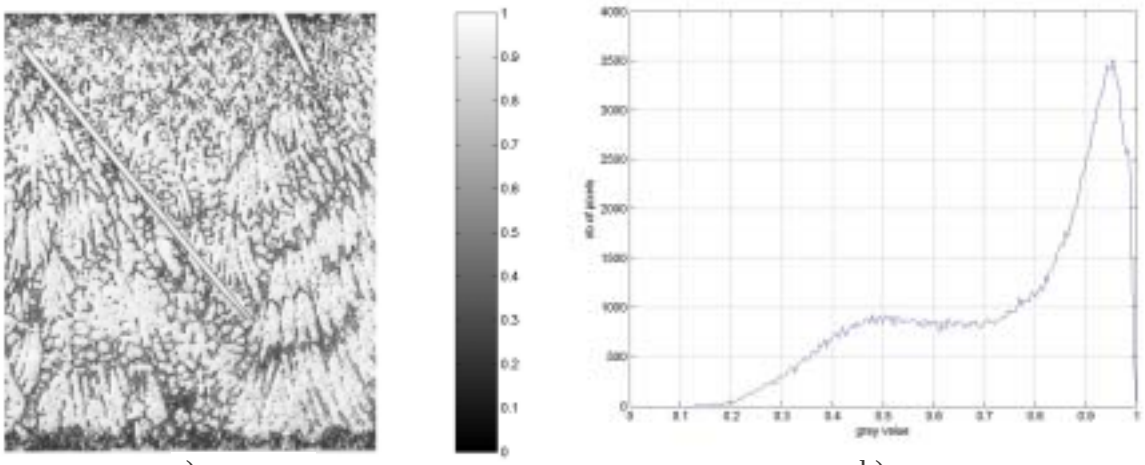

a) b)

Figure 6:The grey image, the greyscale and the histogram (on the horizontal axis are the grey levels, and on the vertical one are the numbers of pixels in the image for each grey level). Grey levels are coded between 0 and 1, at 256 discrete values.

The histogram (Figure 8) was analysed for peaks and a threshold limit was set on the local minimum (dip) in between light and dark peak. For example at the local minimum located at about 0.65 (of greyscale), all pixels left of the threshold are turned into black and pixels on the right were made white.

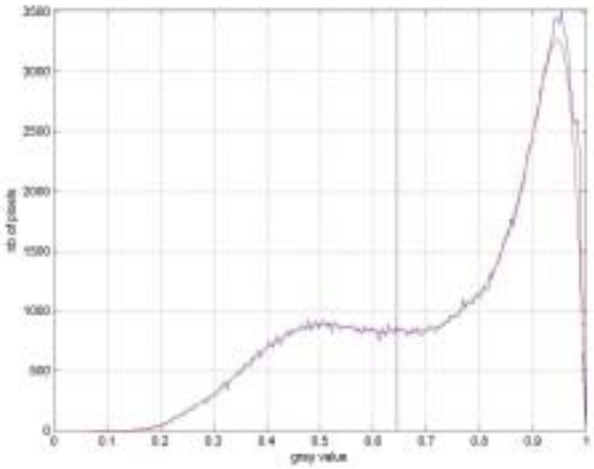

Figure 7: The histogram and the threshold; the red curve is smoothed by cubic splines, in order to detect the local minimum

The resulting binary image is shown in Figure 9. As not all images will generate the same histograms (with a local minimum at 0.65), an automatic threshold method was used. Other commercially available methods can be used such as the Otsu's method [].

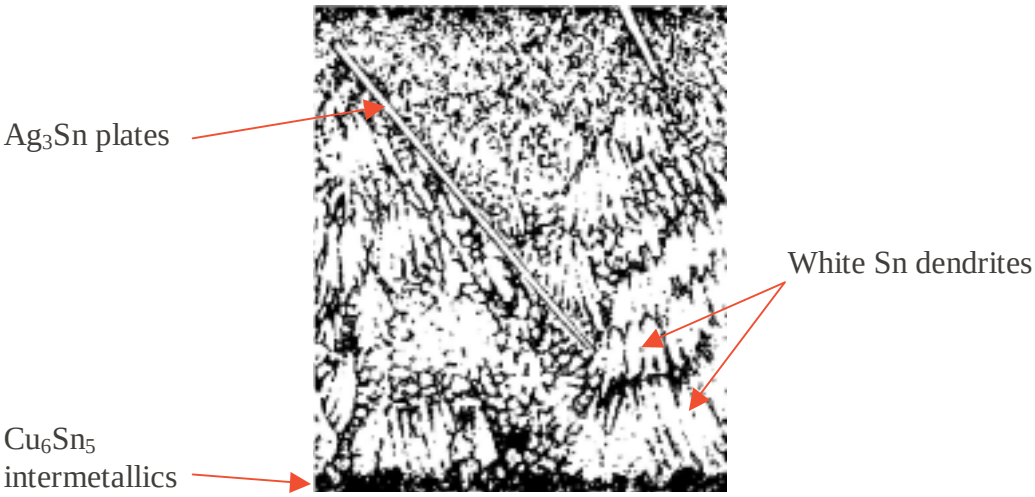

Figure 8: the resulting binary image

Identification of the white and black areas on this binary image; in our sample (M449BGA7 Figures 9) are as follows:

- Black = Lamellae Ag_3Sn in the Sn matrix and the intermetallic layer along interface
- White = Sn dendrites *and* Ag_3Sn plates

Concerning the intermetallic interface, this appears as a solid black area (at the bottom of Figure 9). To extract this feature, and measure its thickness, a process for detecting areas of a common type was used (segmentation).

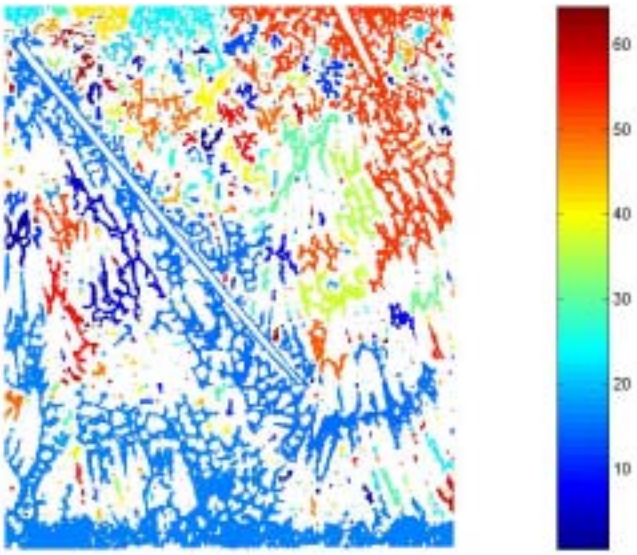

Figure 9 Segmentation of an image into components

In the segmentation procedure a specific area is selected and coloured by the simple rule that adjacent pixels to each other by at least one side of the pixel from either black or white

regions. These connected areas are called ***"components"*** and are indexed with a single number. In our example we have identified 63 components in the image Figure 10.

The intermetallic layer is manually selected, and here is represented by continuous region at the bottom of the image. The average height of intermetallic was calculated by counting the number of pixels in this component and divided by the image width in pixels. A computational approach was largely unsuccessful due to problems in distinguishing between natural tin dendrite structures and that of the intermetallics.

1.3. Intermetallic Flakes

The intermetallic flakes of Ag_3Sn have common characteristic that they appear as either straight lines or flat flakes. By using the Hough transformation straight elements in images can be detected. The basic idea of this transform is depicted in Figure 11. Assuming there is a blue straight line in the image, usually defined by its slope and its intersection with the y-axis. However, we can also describe this line with its perpendicular distance r_0 to the origin, and the angle θ_0 between r_0 and the x-axis. Therefore, the original straight line is now a point in Figure 10b).

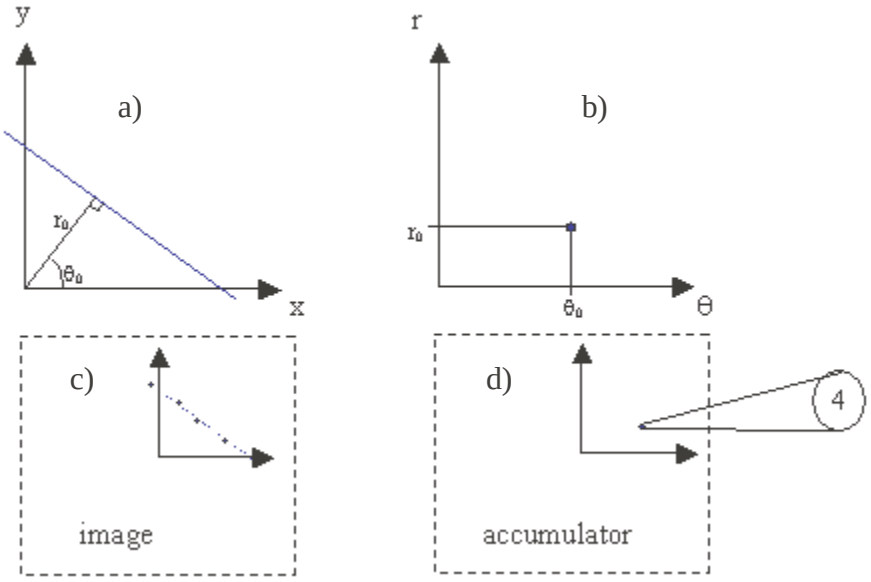

Figure 10 Description of the Hough transform

A typical algorithm that uses this transform is the following: each time a white pixel is encountered on the dotted line in Figure 11c), the accumulator is incremented at the line coordinates. For instance, in Figure 10c), the blue line is made of four adjacent pixels with the centres marked, the value of the accumulator is therefore 4 at coordinates (r_0, θ_0) shown in Figure 10d). Thus the longer the line, the higher the value in the accumulator. The Hough transformation only works on edges or lines, so to use the transform, Figure 9 must be converted with an edge detection algorithm, as shown in Figure 12.

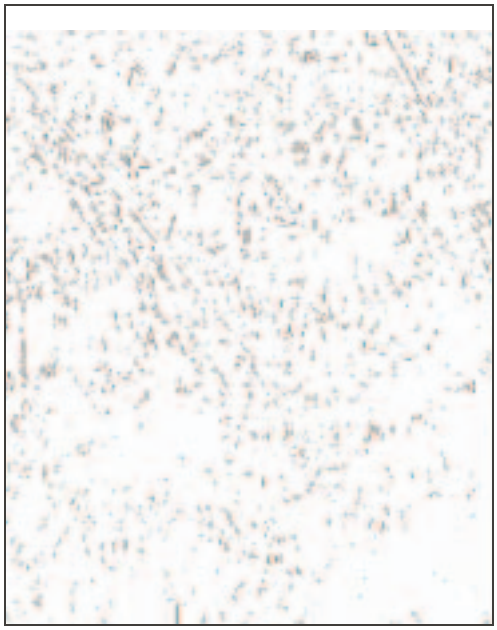

Figure 11 The image (Figure 9) converted with edge detection algorithm

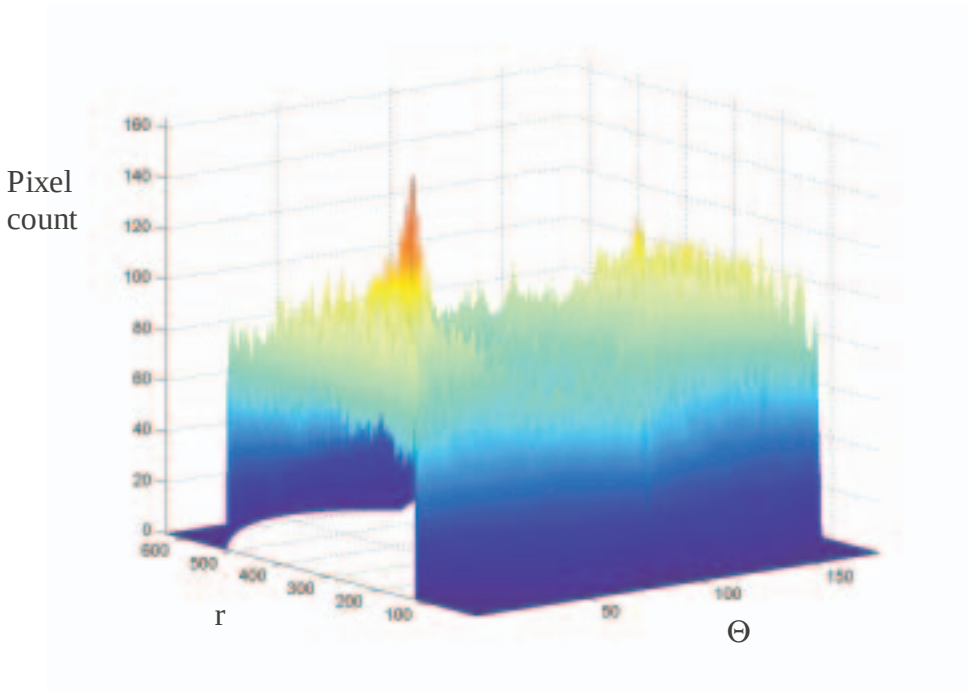

Figure 12 3 D plot of accumulator for figure 11

Figure 12 is a 3D visual representation of the accumulator matrix and shows a clear peak corresponding to the long Ag_3Sn intermetallic.

Figure 13 shows an overlay of the identified peak coordinate (i.e. line characterized by coordinates (r, Θ) and the original image, which shows that the algorithm is working.

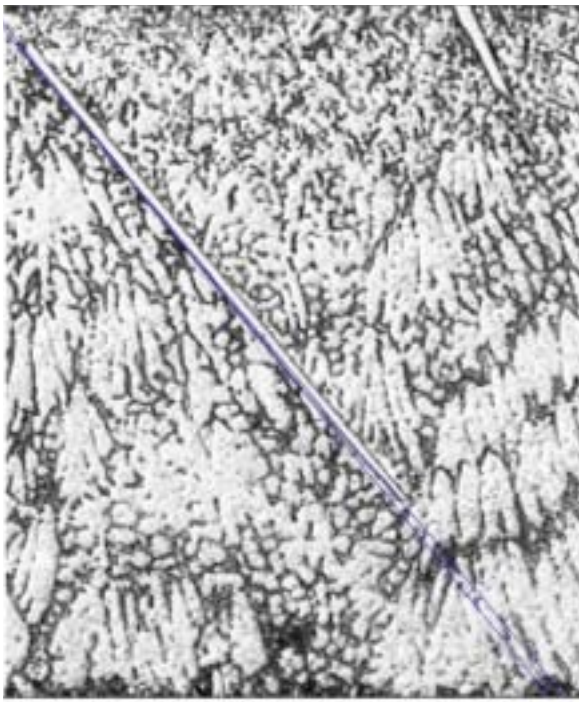

Figure 13: Confirms by plotting overlay of the r, Θ back onto the Figure 8 showing

Having identified the flakes, when present (which is a function of the microsection) we now consider the tin dendrite structure.

1.4. Detecting Fine and Coarse Structures of Dendrites

Here we attempt to size the original white tin dendrites as can be seen on image M429BGA5 (Figure 8), we can distinguish a fine structure of dendrites at the top of the picture and a coarse structure at the bottom. The strategy is to remove the areas where the dendrite direction cannot be determined.

The method is to characterize the dendrite size throughout whole image. The approach is to draw random lines across the image, see Figure 14 and to record the length of continuous white or black pixels along the line this is plotted in Figure 15. These lengths are then plotted in a histogram, in Figure 16 and peak position recorded. This peak, se Figure 16 is the average length of white-pixel peaks, i.e. the average length without crossing a black pixel this parameter characterizes the size of dendrites.

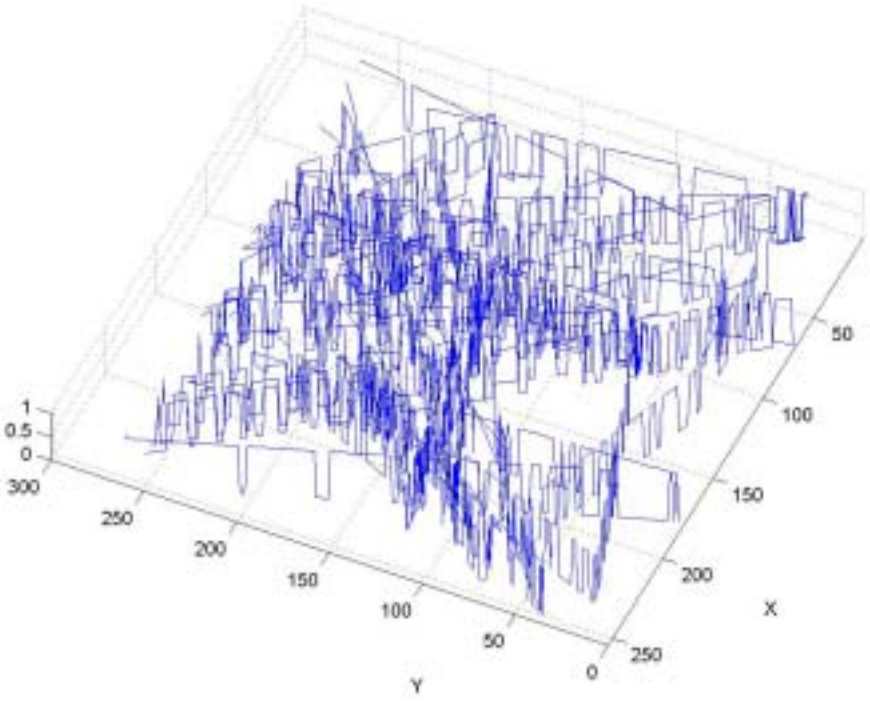

Figure 14: the random path across a binary image; the intensity profile value is represented in 3D between 0 and 1.

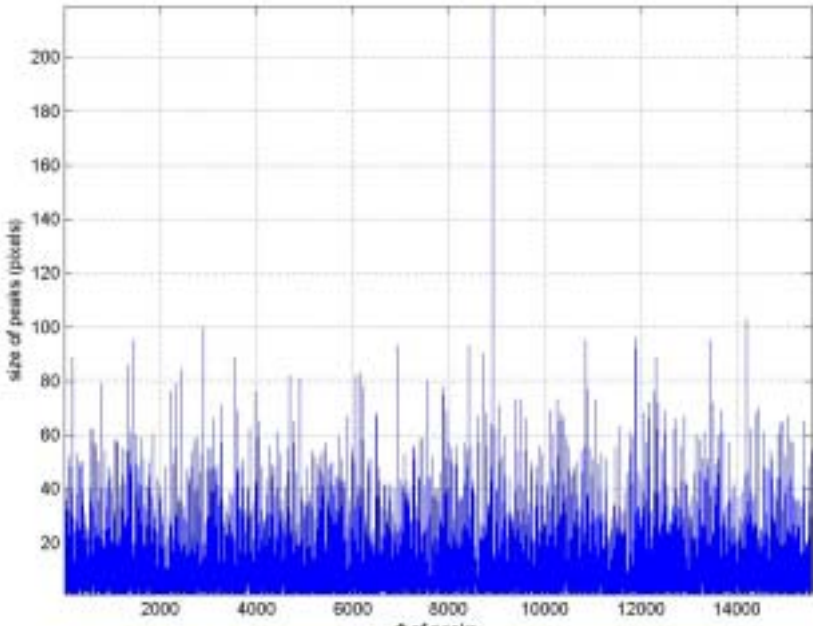

Figure 15: plot representing the length along the path of each white peak; for example, the peak #3000 about ~ 100 pixels length.

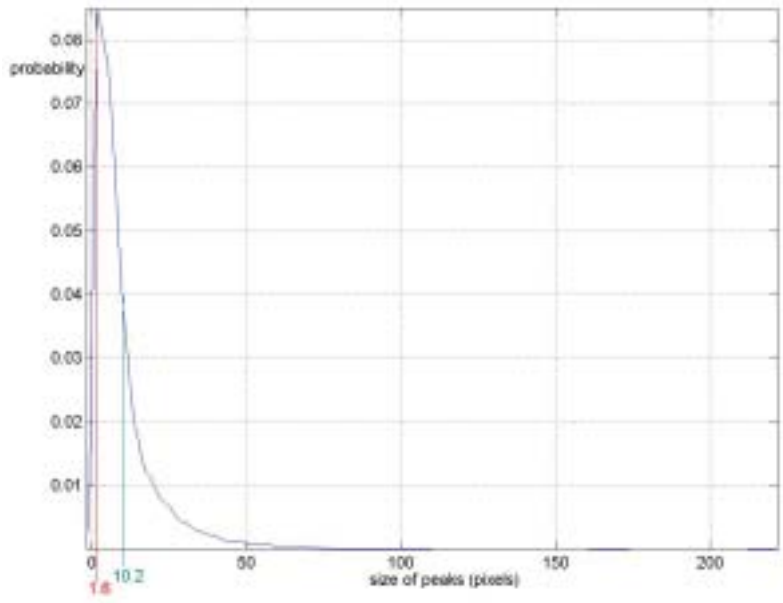

Figure 16: Probability density function of peak sizes. 1.6 pixels peaks are more likely to occur, and the mean size of peaks is 10.2 pixels (1 pixels ~10μm)

This approach must actually be applied on a small scale to get useful measurements, and then move this analysis area over whole image in a step-wise fashion. The random profile is run over a mask of 5x5 pixels and the result (the mean length) is stored at the centre pixel position in the output matrix, the mask is sequentially moved across the image repeating the procedure.

There are two options in the moving the mask:

1. Move by mask size, generating a course map
2. Move mask by a single pixel, generating a fine map

Figure 19 shows the result of using the fine map approach.

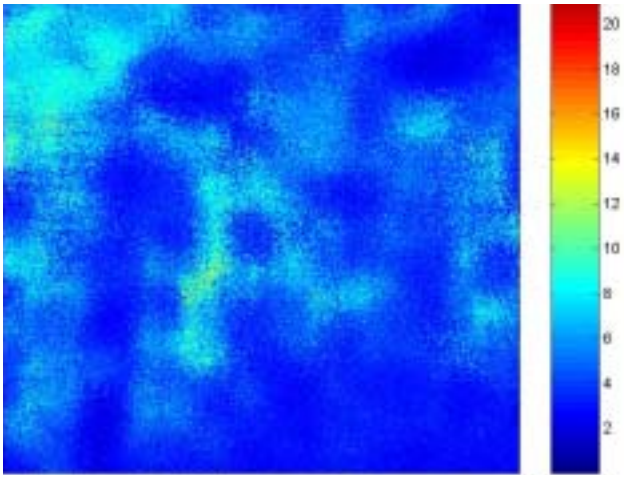

Figure 17 top left: original binary image, top right: coarse map of average lengths of white peaks across the image (mask = 51), bottom left: fine map (mask = 51)

On these two types of image, it is not easy to apply an efficient threshold to separate the fine and coarse structures. Another function has been developed, which aligns these two maps,

using a weighted average between the values and the following was found to give the best results:

- the fine profile weights as 2
- the coarse one weights as 1

The result is shown below (Figure 18). In Appendix II you can find other maps with different weights for the same image.

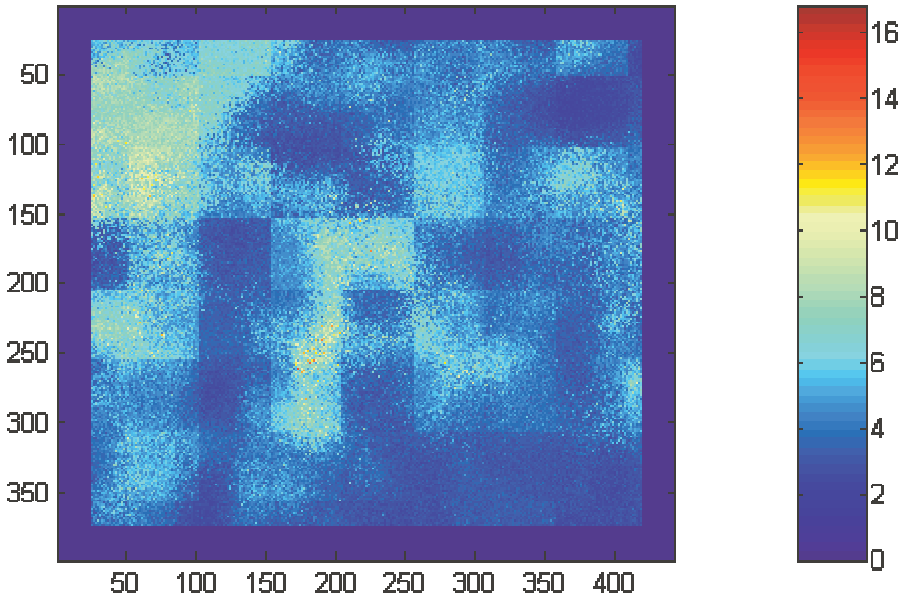

Figure 18: weighted average between the coarse and fine profiles

Then it is possible to apply a threshold to this map, in order to separate fine and coarse structures; this is a result with a threshold value of 5 pixels (Figure 19):

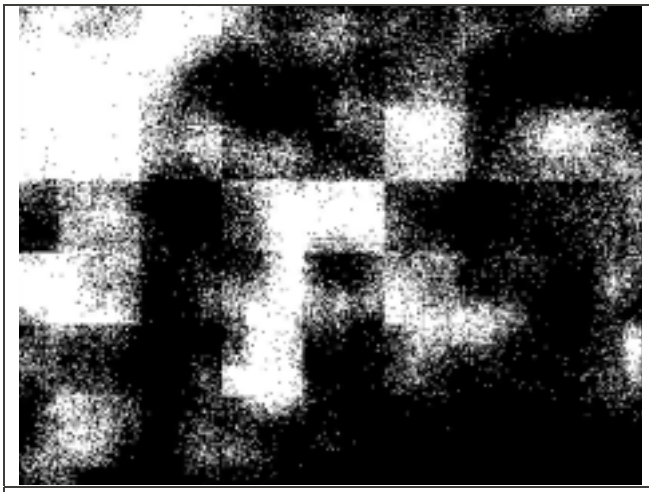

Figure 19: binary map after application of a threshold of 5

Figure 20: the corresponding coarse area on the original image

After some tests, the value of 5 pixels seems to be here the optimal mask size. The Figure 19 is multiplied by the original image to give Figure 20, and we can now clearly see large dendrites in this area. The next step then is to measure the dendrite orientation and size.

1.4.1. Detecting dendrite direction

Microsections of tin rich alloys typically form a number of colonies at random orientations. Within any one colony the dendrite has a characteristic feature size for all the dendrites, where this feature maybe the length or width of the dendrite. Therefore, by identifying the orientation of the dendrites, the colonies are identified and hence the dendrite measurement technique can be applied to each colony.

This method used has common characteristics with the previous one, and is described trough an example in Figure 21:

- white dendrites oriented north-east / south-west. The goal is to detect that direction.
- in blue there is a set of diameters in a circular shape, with a one-degree increment.

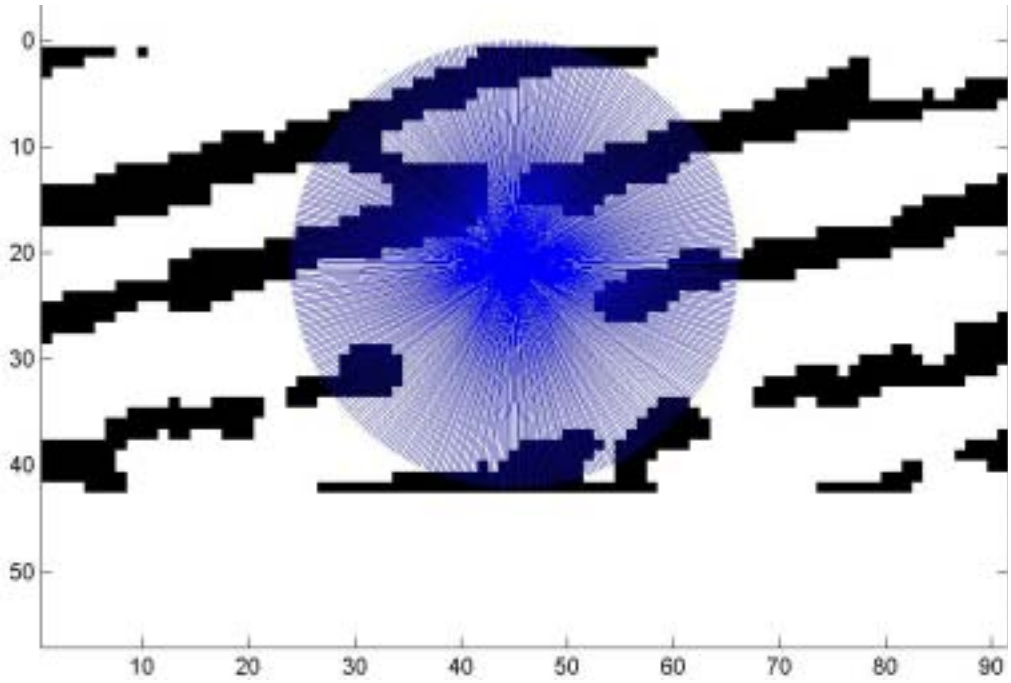

Figure 21: the new circular shape profile to detect dendrites directions

With each line in the circular set, the following algorithm is performed:

- if the centre pixel is white, the percentage of white pixels on the line is returned
- if the centre pixel is black, the percentage of black pixels is given.

The distribution of lengths (white or black pixels) for each angle is plotted in Figure 22. Later the origin of this circle (a sampled cell) will be moved in an incremental fashion throughout the image.

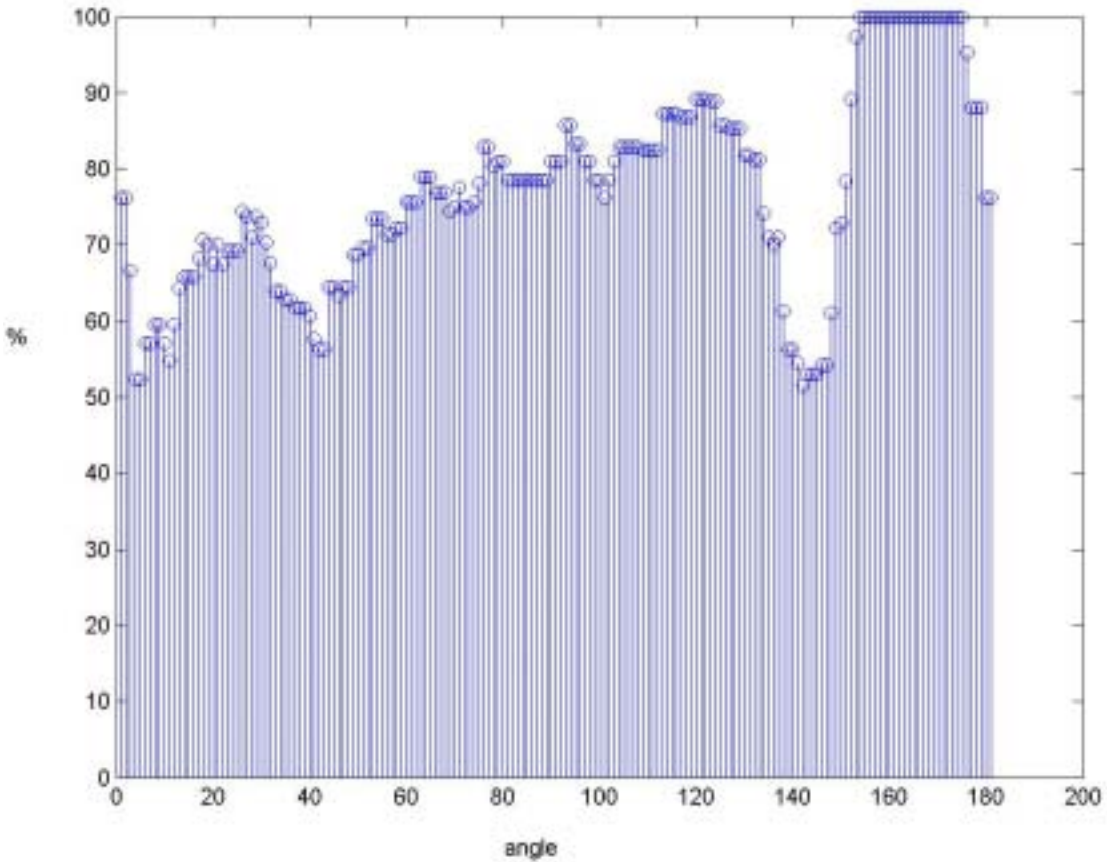

Figure 22: percentage of white pixels according to the angle of the line with the Figure 34 example

In a region of 155-178° several full white lines are observed, and confirms the identity, i.e. Figure 21 the unique direction of the dendrite. The final direction is calculated as a median of angels with 100% black or white pixels.

- first we extract the angles of fully white lines
- we plot then the probability density distribution of these angles: the maximum gives the most likely direction of dendrites:

Then the method is applied as an operator through the binary image, as previously described, and at each sampled cell, a line is plotted about the cell centre to indicate the calculated dendrite direction. An example test run on an artificial test image is shown in Figure 24.

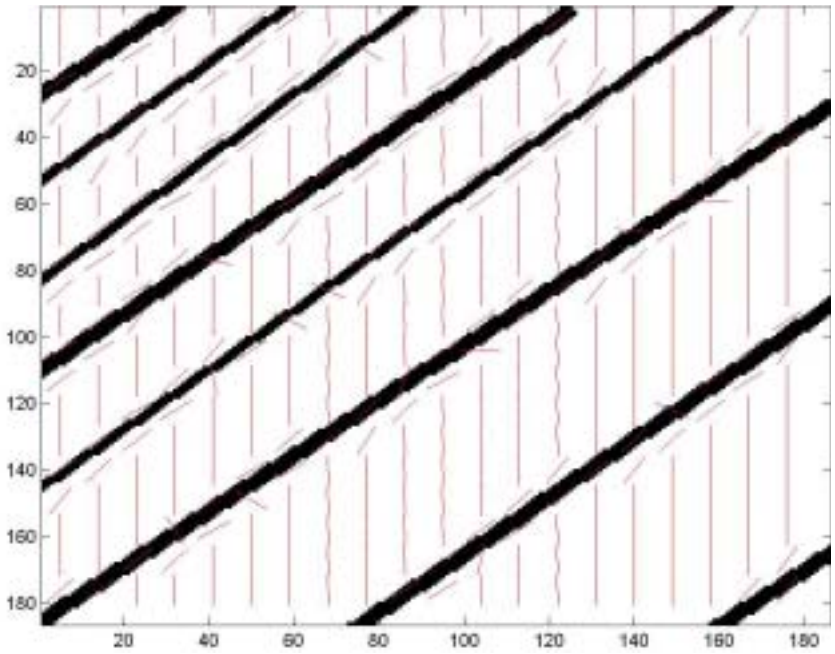

Figure 23: test of orientation detection, with a trial image

This test highlights a drawback on monochromatic areas (here, white areas): the default choice is the vertical direction; to correct this phenomenon, when the area covered by the mask is monochromatic, the left-hand orientation is copied to the current one, the new result is seen in Figure 25.

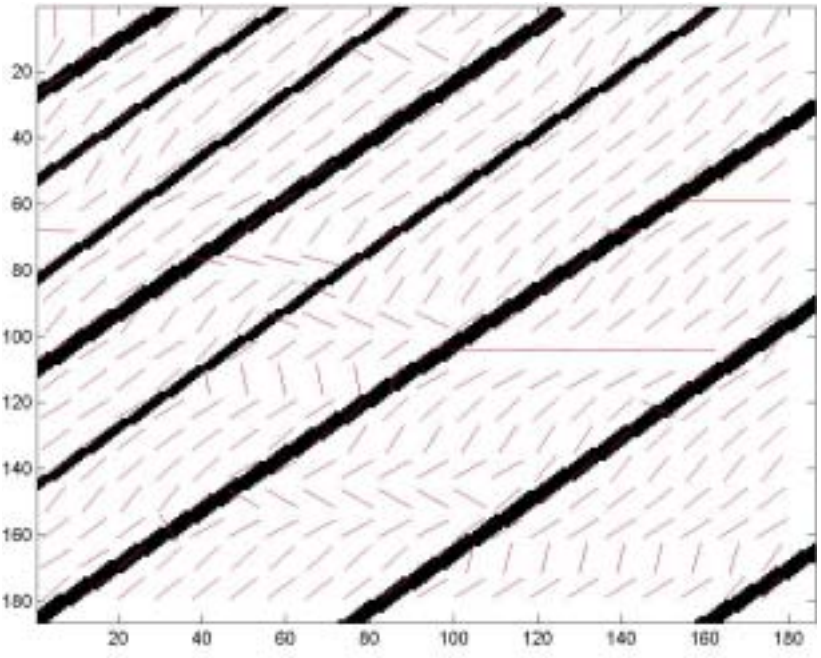

Figure 24: illustration of the correction on monochromatic areas

The overall match now is far superior to that of Figure 24, although approximately 10% of the estimates of the orientation do not fit the actual direction, and the wrong result is copied in the following cells.

The method was applied to a microsection and the result of dendrite orientation is marked in Figure 26..

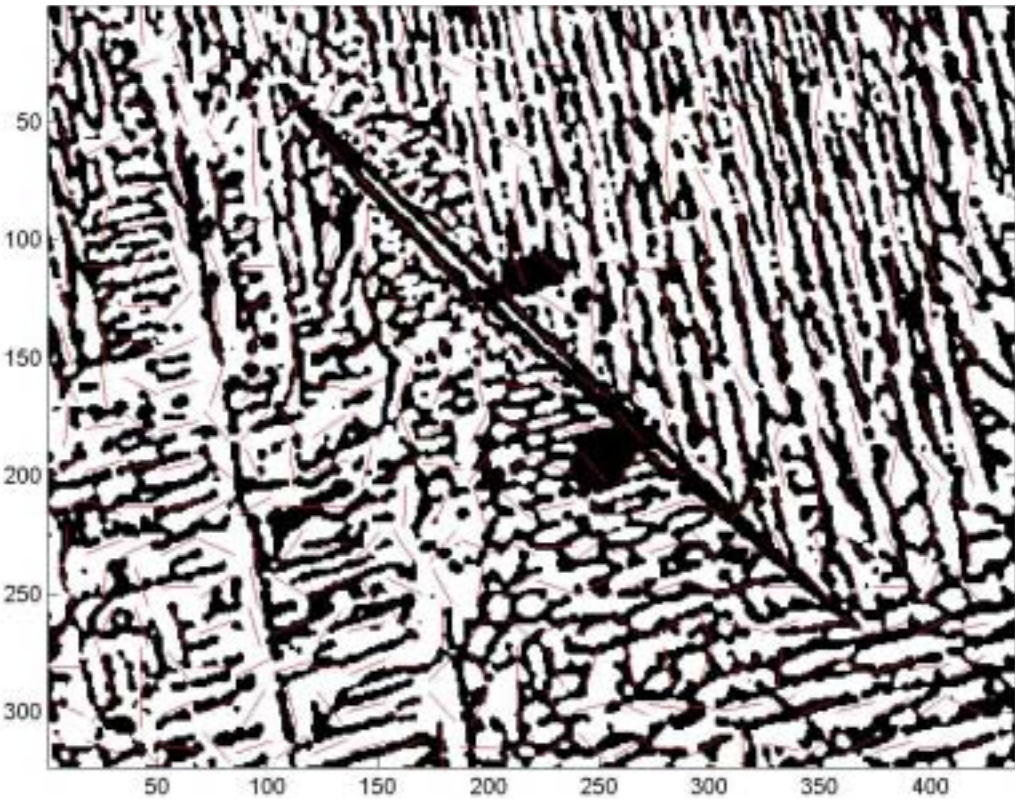

Figure 25: orientation detection on a binary sample image

In Figure 28 the size of the applied mask was 17x17 pixels. In Appendix III there are pictures processed using masks ranging from 11 to 25 pixels and the processing times. The 17-pixels mask seems to be here the best compromise between resolution, accuracy of results and computing time.

To digest the orientation information the distribution from each cell can be plotted in a histogram (Figure 27), in order to determine the most common dendrite orientation in Figure 26.

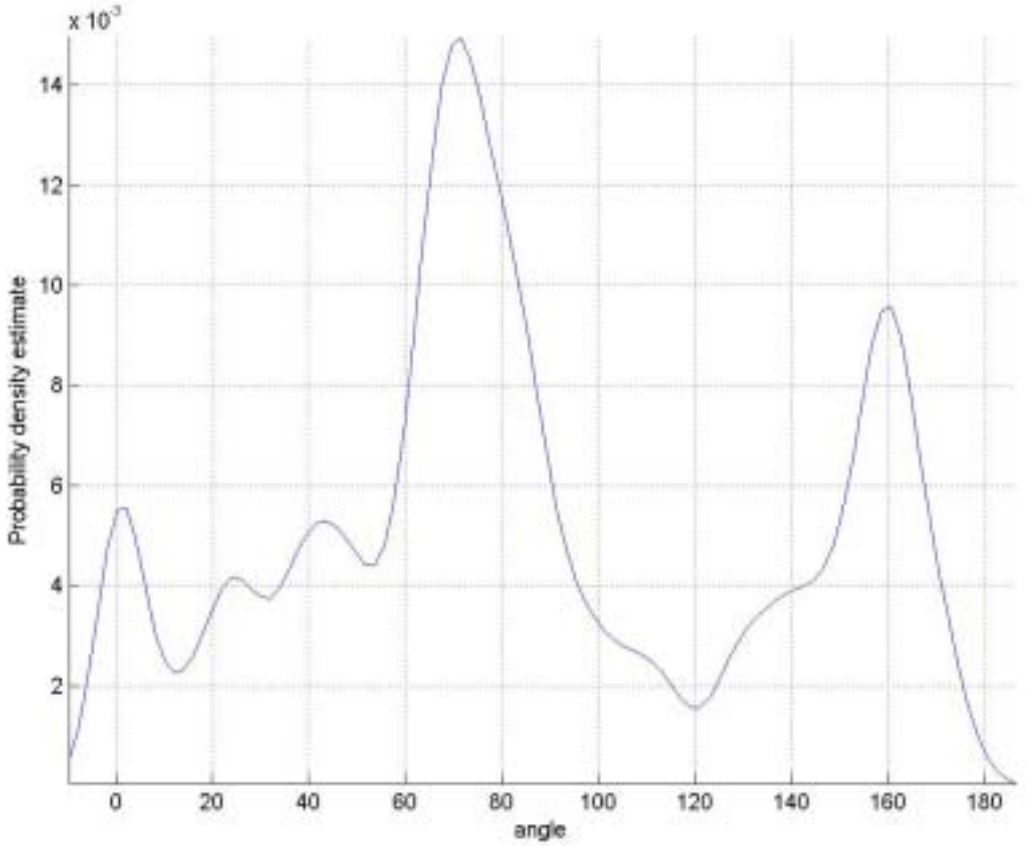

Figure 26: probability density estimate of the number of lines in respect with their direction

From this graph, it is possible to specify ranges of angles, in order to work out classes of dendrites with common orientation. Each class is then assigned a colour, which is reproduced and overlaid on top of the original image in Figure 26. From this graph classes of specific orientations of dendrites can be associated with the various peaks.

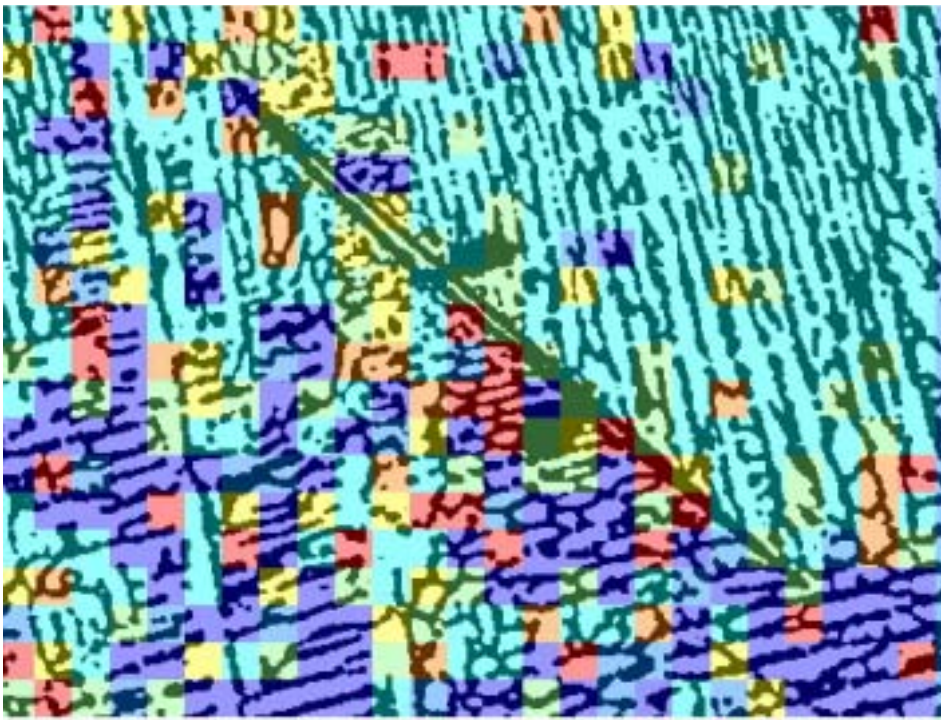

Figure 27: On this picture, each color is a class; light blue blocs are oriented at about 70°, dark blue ones are 160°, etc...

In order to determine classes in an automated fashion each local minimum was detected in the distribution (Figure 27), and then a class was associated with matching interval, as shown on Figure29.

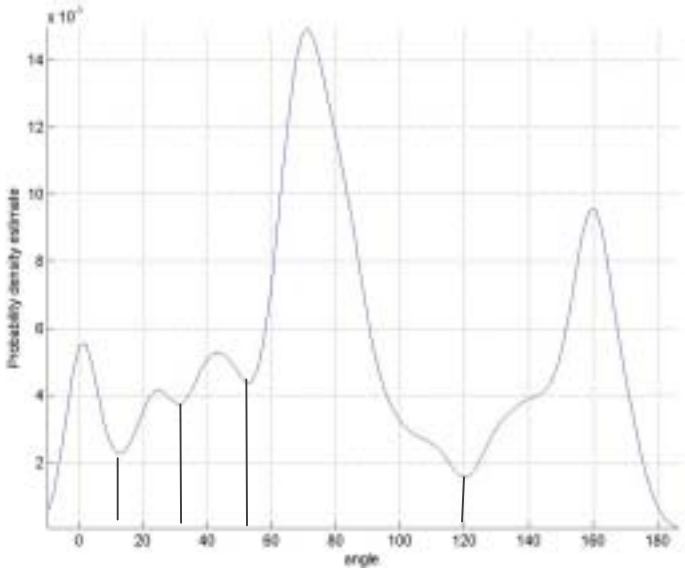

Figure 28: each local minimum is the border between classes (5 resulting classes)

However, it seems that this approach produces too many classes, as shown in Figure 30. There are too many classes with only a few elements inside. To simplify the image and reduce the number of classes the selection of peaks can be modified.

To reduce classes the following process is applied (see Figure 30). The minimal class-range is reduced and replaced by a boarder between two consequent classes. The border lies at the mean value of the class being reduced.

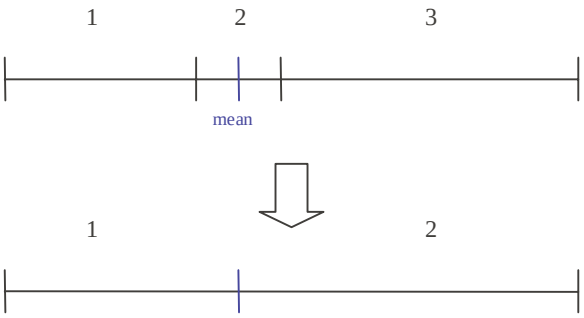

Figure 29: how to shift from three to two classes

The results with a 17-pixel mask are shown in Appendix III, with a number of classes comprised between two and five.

Another method to reduce/eliminate the number of classes is to allow a user to select peaks directly from the distribution plot, as depicted in Figure 31. The remaining intervals are kept white as well as the unrecognised directions of dendrites.

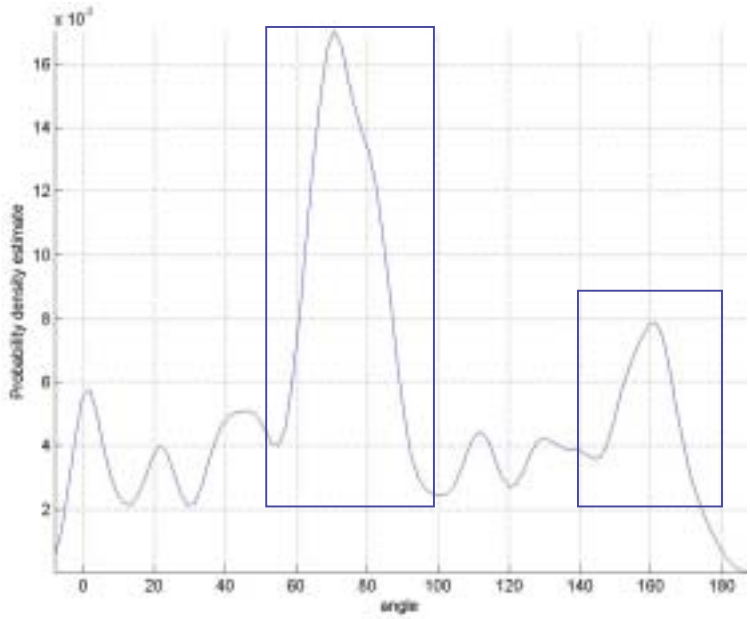

Figure 30: the user selected 2 classes: [50° 100°] and [140° 160°]

The result of this selection is shown in Figure 32.

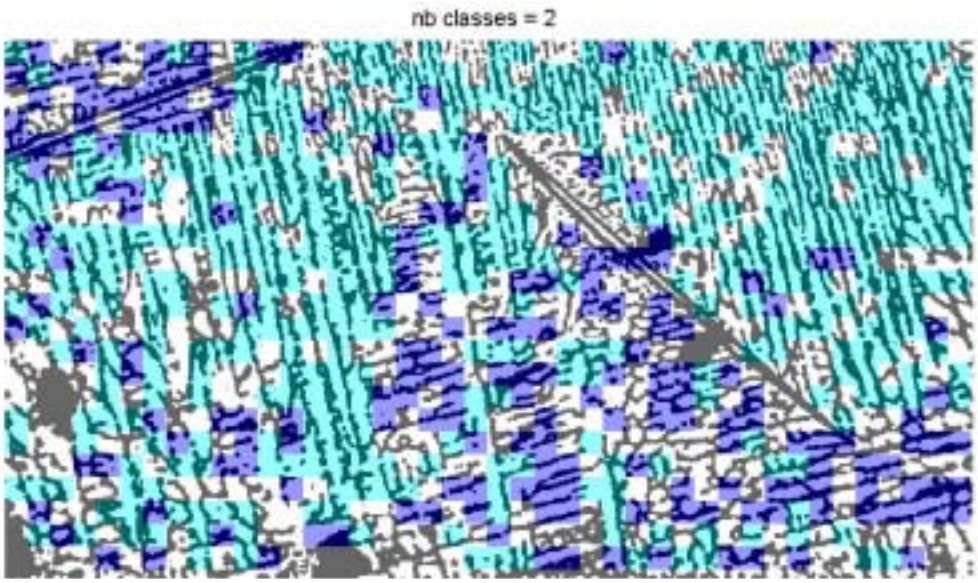

Figure 31: only two user-selected classes are left; other blocs are left blank

However, a drawback of this method is that grains with the same direction will be considered to belong to a unique class, as shown on the previous picture (Figure 34): only one class is detected for grains on the right and the left of the sample.

Furthermore, for each class, the "random profile" method has been applied on the masked image, in order to give a measure of the size of dendrites within each class. The results are given as distributions plots in Figures 35.

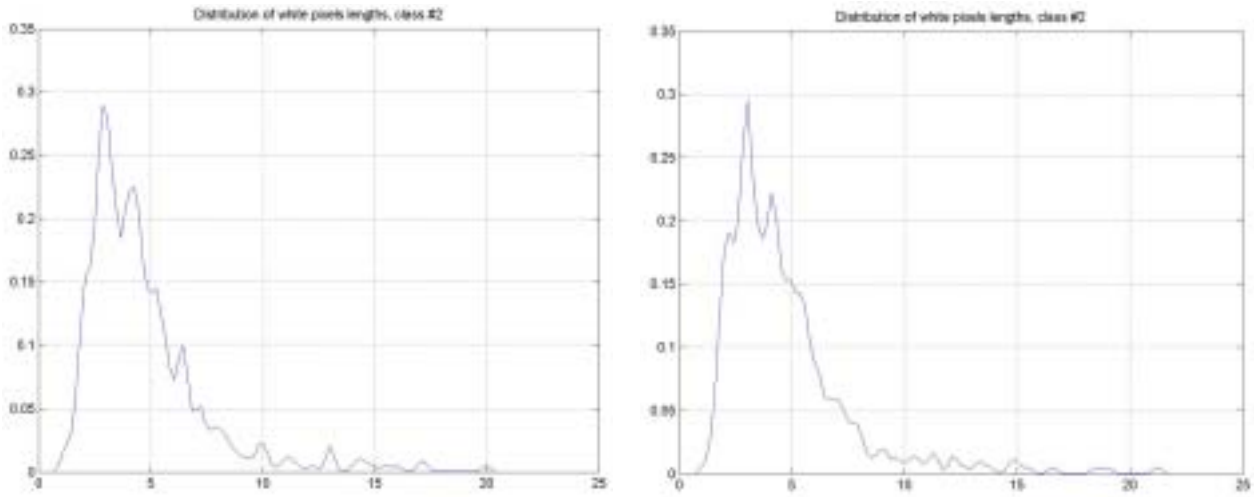

Figure 32: two trials of distribution plots for the same class (light blue); means are 46.8 µm

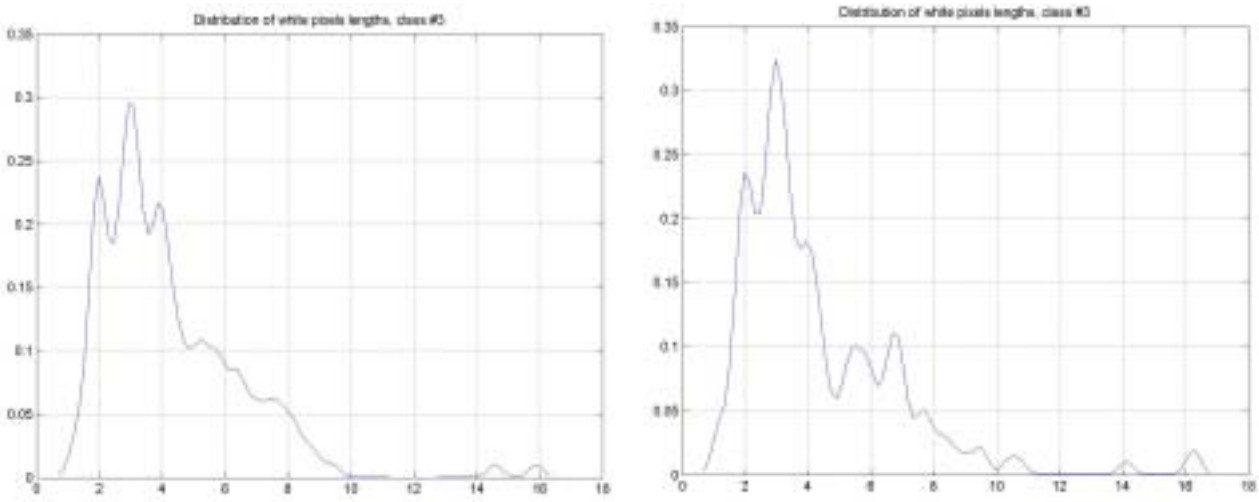

Figure 33: the same for the dark blue one; means are 42.1 and 43.0 µm

This shows that the method is quite robust; the values of curves remain quite the same for each trial, and the general shape of distribution is maintained.

To confirm that, several trials were performed and white peak average values were collected for two classes:

Trial number	Class #1	Class #2
1	4.070	3.918
2	4.071	4.004
3	4.102	3.936
4	4.076	3.914
5	4.145	3.891
6	4.132	3.867
7	4.069	3.980
8	4.132	3.877
9	4.154	4.043
Mean	4.106	3.937
Standard deviation	0.035	0.060

However, for best results, this method should be applied on coarse structures only, i.e. after having processed the detection of coarse and fine structures (see Figure 22). The quality of results highly depends on the success of the previous step that splits the image into classes.

2. Conclusions

The best results can be achieved following these recommended steps:

- concerning the intermetallic flakes, texture analysis results should be analysed further, and gathered with Hough transform based method;
- detection of dendrite direction should be applied only on coarse structures;
- voids have not been treated; consequently the user has to select an area without these;
- Cu_6Sn_5 elements have not been taken into account, for SAC solders

If the requirement is to characterise microstructure features objectively

A main drawback of some developed functions is the processing time, which can reach an hour for one image. This may be due to the use of Matlab with loops, whereas this software is designed to work on matrixes. Thus, the use of C language may be an improvement for some functions.

Documentation work represented a significant part of the work. Indeed the functions will be used only if they are clearly documented. Furthermore, the programmer's documentation can help in future improvements.

The aim of this project was to provide the ability to characterise some features of the microstructures, in respect with the environmental experiment conditions. These numerical results will be gathered in order to contribute to the analytical model and mechanical properties measurements. Consequently, this will contribute to better understanding of reliability of lead-free solder joints.

3. References

[1] Frear, D.R, Jones, W.B., Kinsman, K.R.: Solder Mechanics, A State of the Art Assessment, TMS 1990, ISBN 0-87339-166-7

[2] NPL weblink: http://www.npl.co.uk

[3] Electronics Interconnection Group: http://www.npl.co.uk/ei

[4] MPP5.2 Lead-free Project: http://www.npl.co.uk/ei/research/mpp52.html

[5] NPL Intranet

[6] H. Bässmann, Ph. W. Besslich, Ad Oculos Image Processing, DBS, 1993, 252 pages

[7] S. O. Dunford, A. Primavera, M. Meilunas, Microstructural evolution and damage mechanisms in Pb-free solder joints during extended -40°C to 125°C thermal cycles. On IPC Review vol. 44 N°1, January 2003, p. 8-9

[8] J. S. Hwang, Environment friendly electronics: lead-free technology, Electrochemical Publications, 2001, 879 pages

[9] M. McLean, Directionally solidified materials for high temperature service, The Metals Society, 1983, 337 pages

[10] Campbell, J.: Castings, Butterworth-Heinemann, 1991, 288 pages

4. ACKNOWLEDGEMENTS

The authors are grateful for the support of the DTI as part of its MPP Programme, and of Goodrich, DEK Printing Machines, ESL. The authors are also grateful to Brian Richards and Martin Wickham for useful discussions throughout the work.

Appendix I: Tests of weights for coarse and fine profiles

- Fine and coarse profiles have the same weight: 1 :

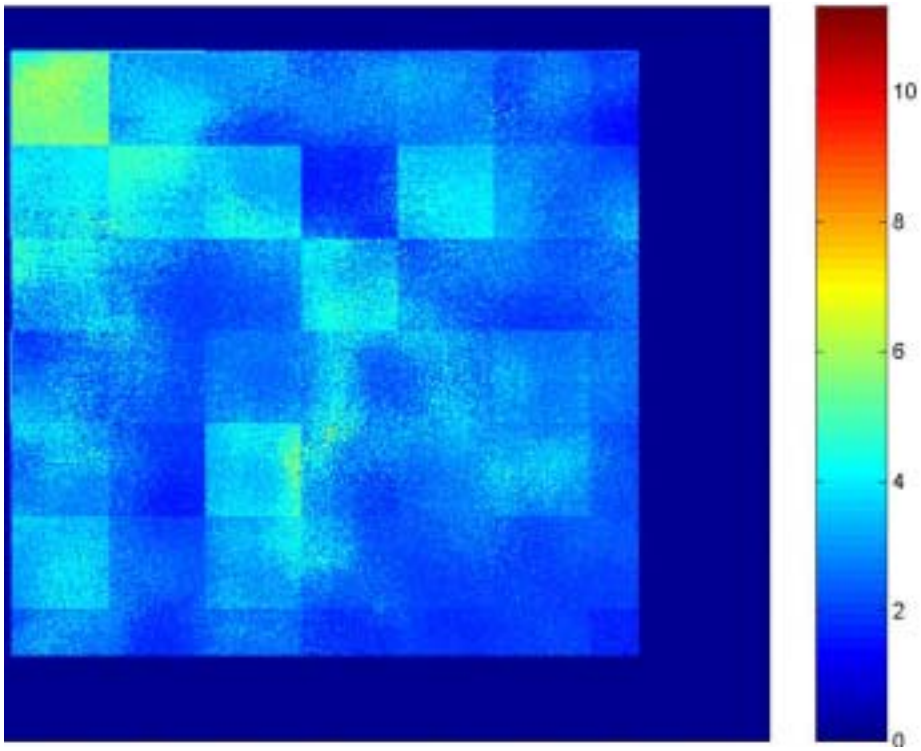

- Fine profile weights as 1 and coarse one as 2 :

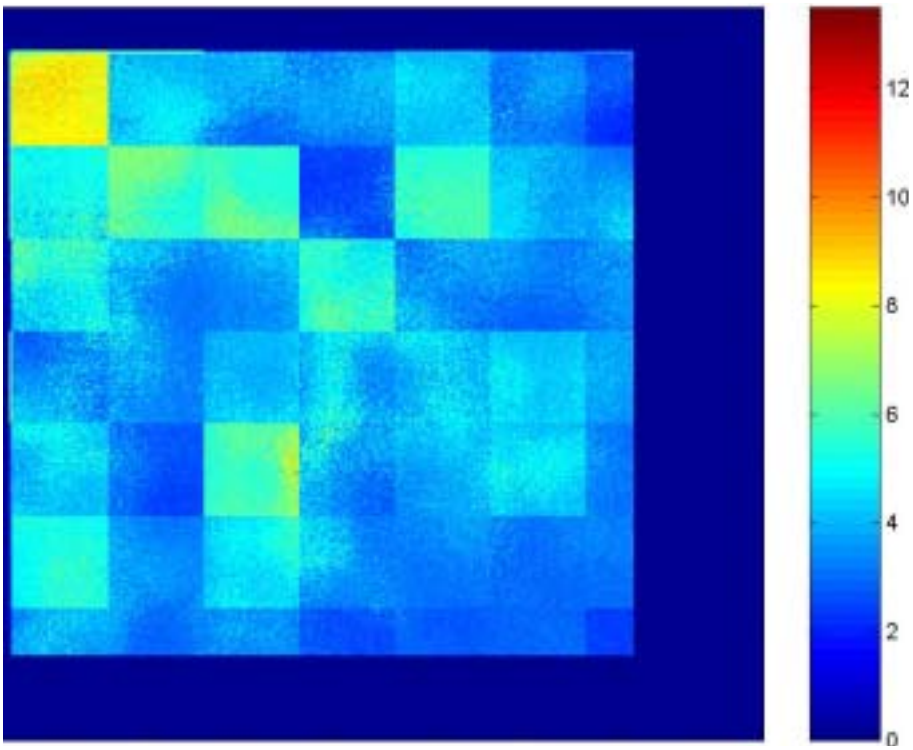

Appendix II: directions maps and results of automatic classes determination

- Mask = 9, 980 seconds, 6 classes :

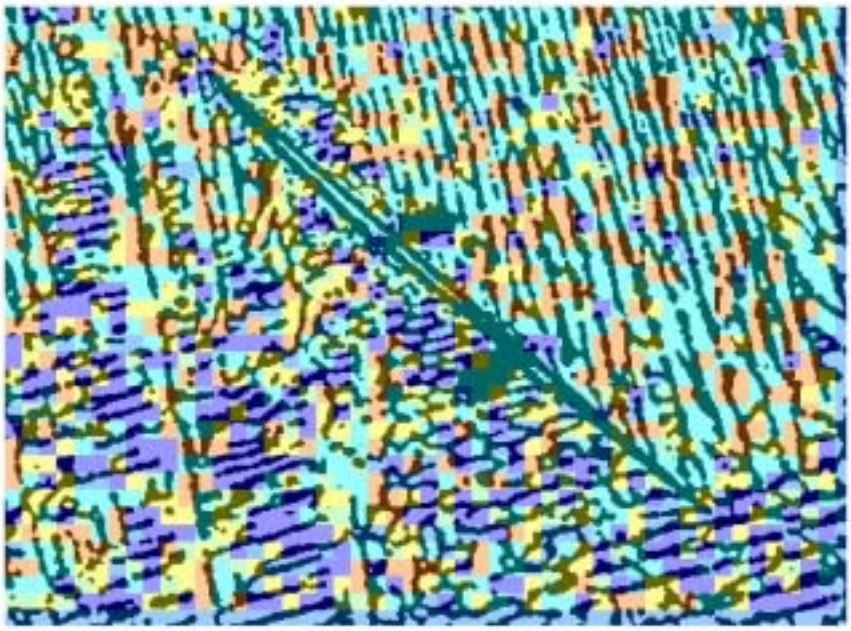

- Mask = 11, 655 seconds :

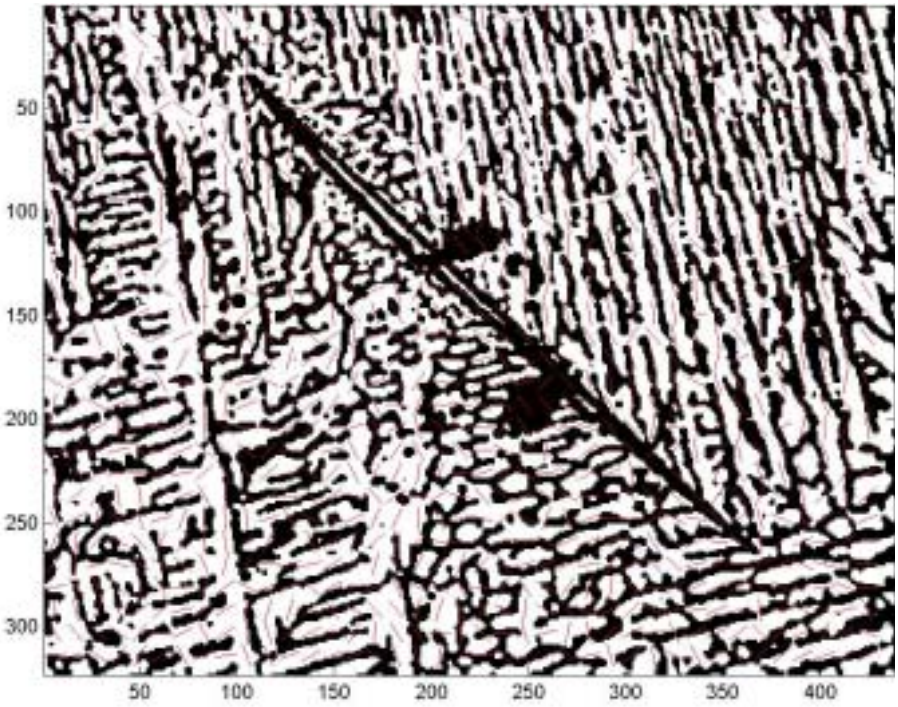

- Mask = 11, 5 classes:

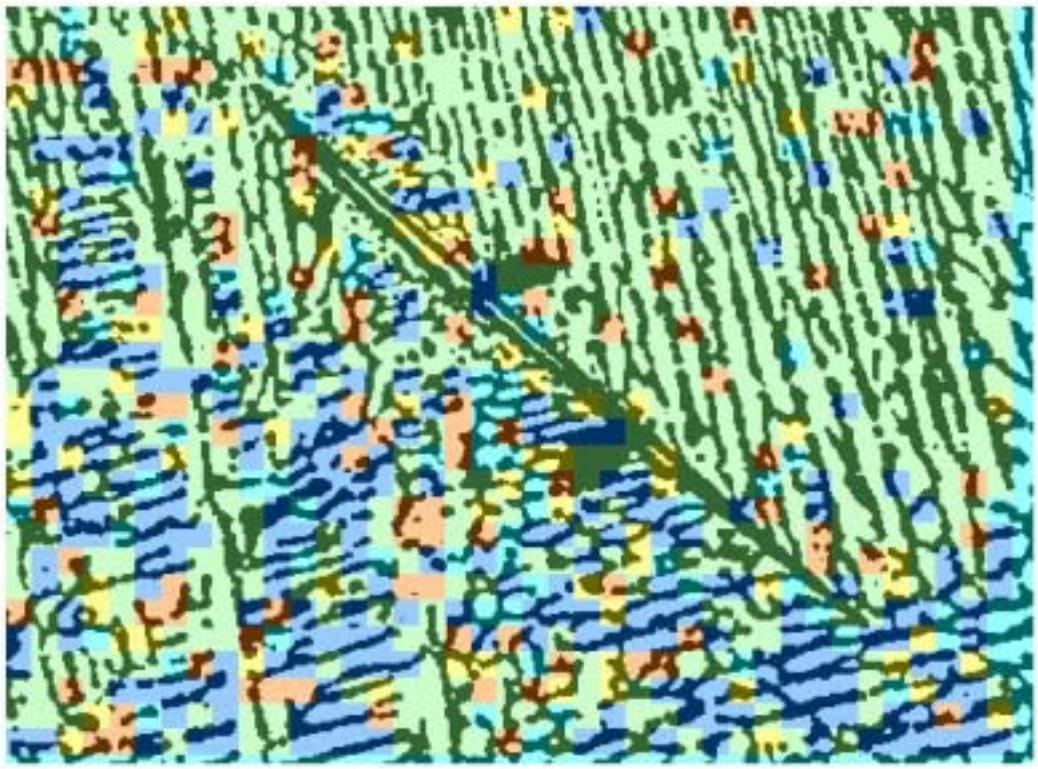

- Mask = 13, 460 seconds:

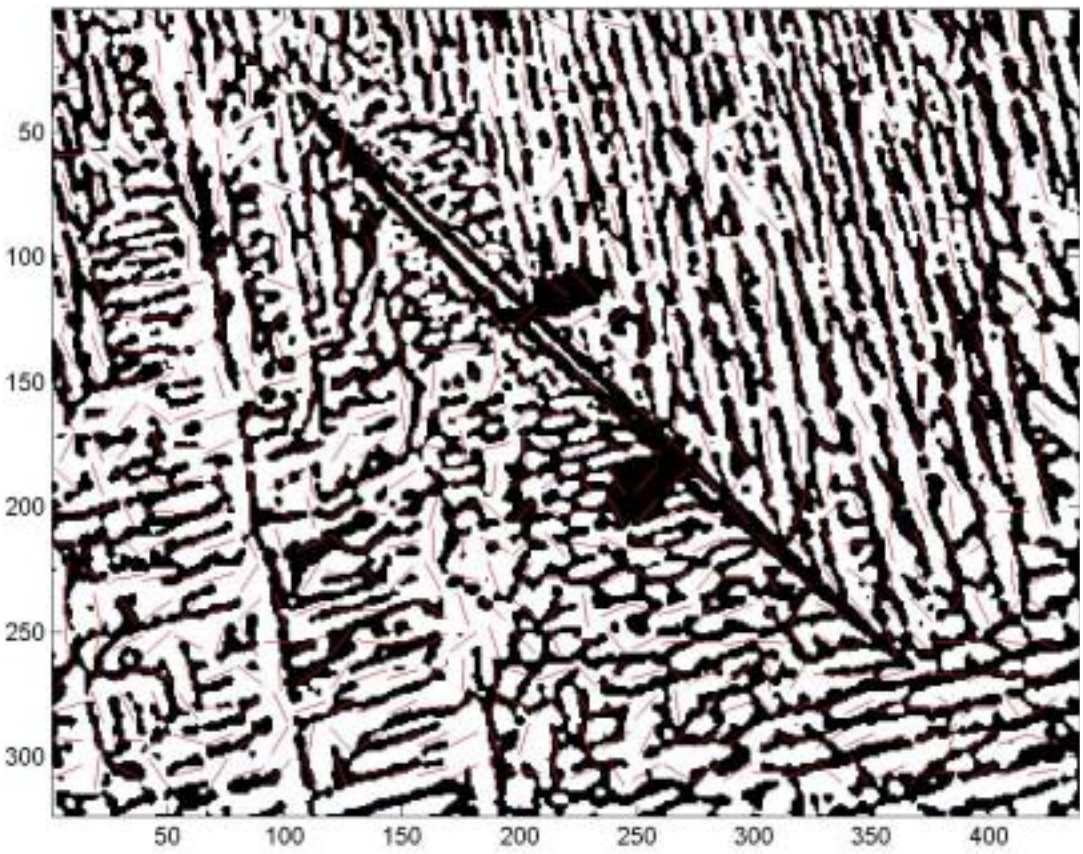

- Mask = 13, 6 classes:

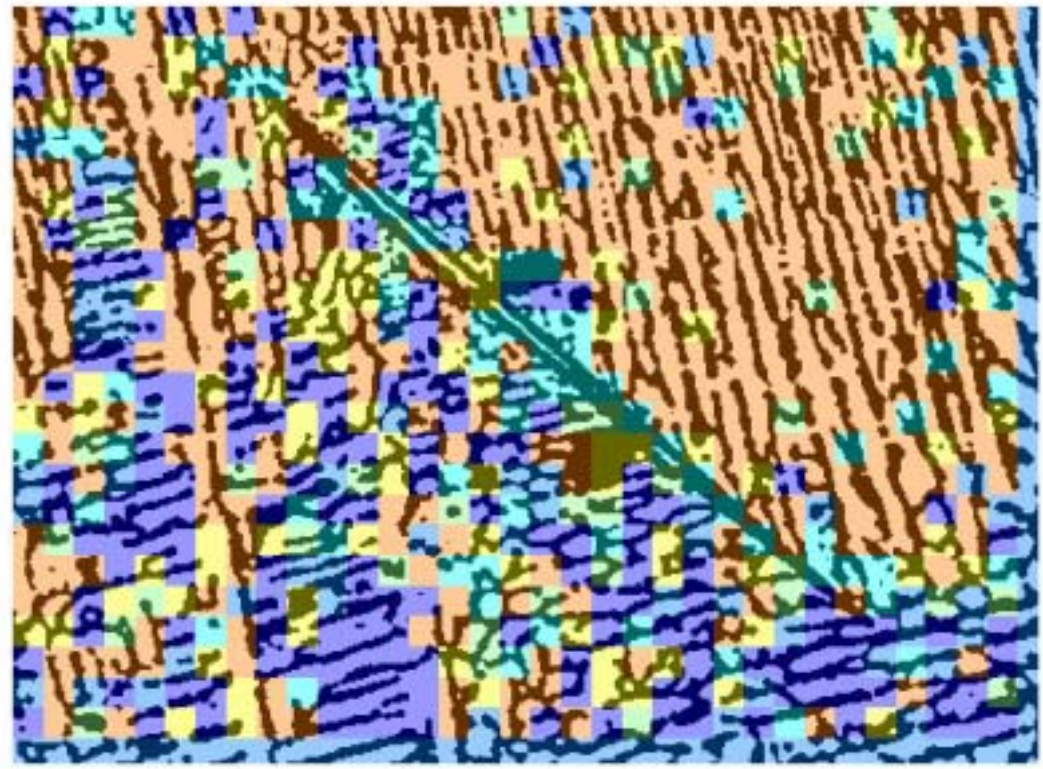

- Mask = 15, 350 seconds:

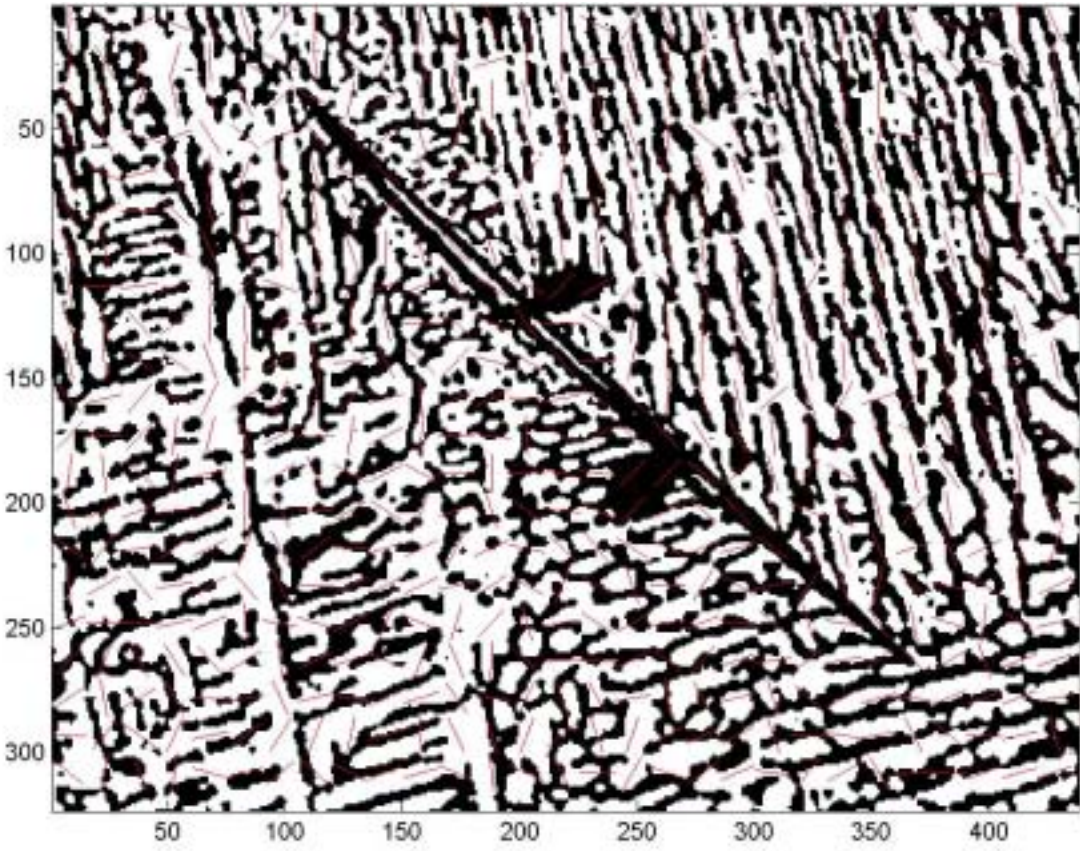

- Mask = 15, 6 classes:

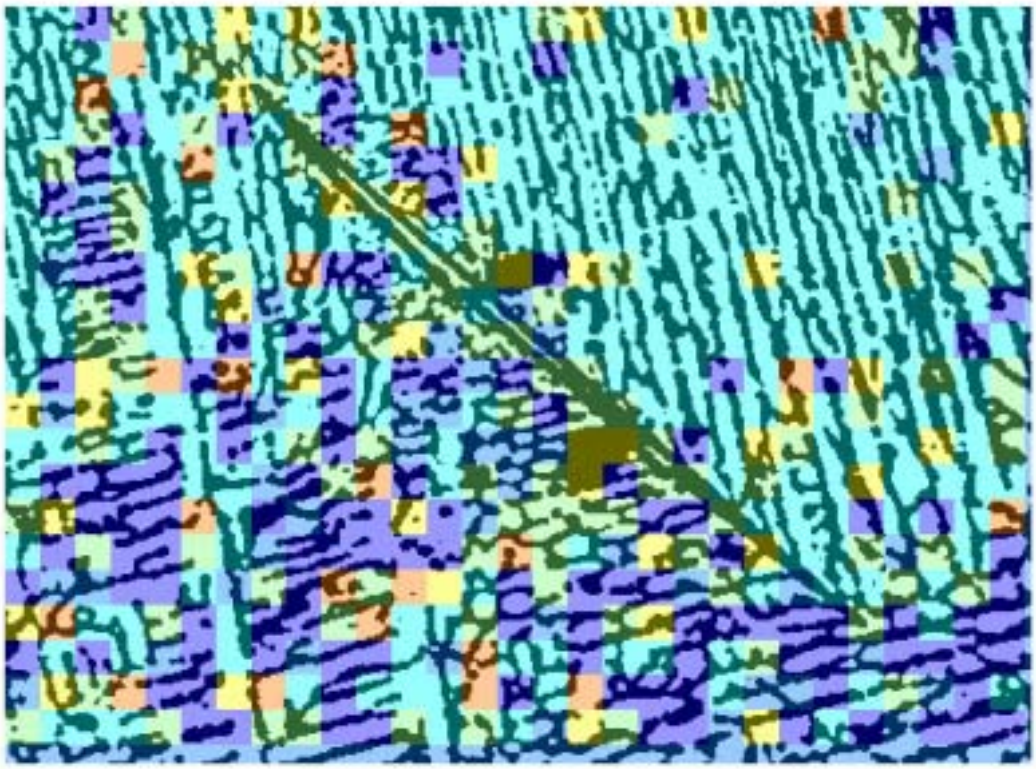

- Mask = 21, 190 seconds:

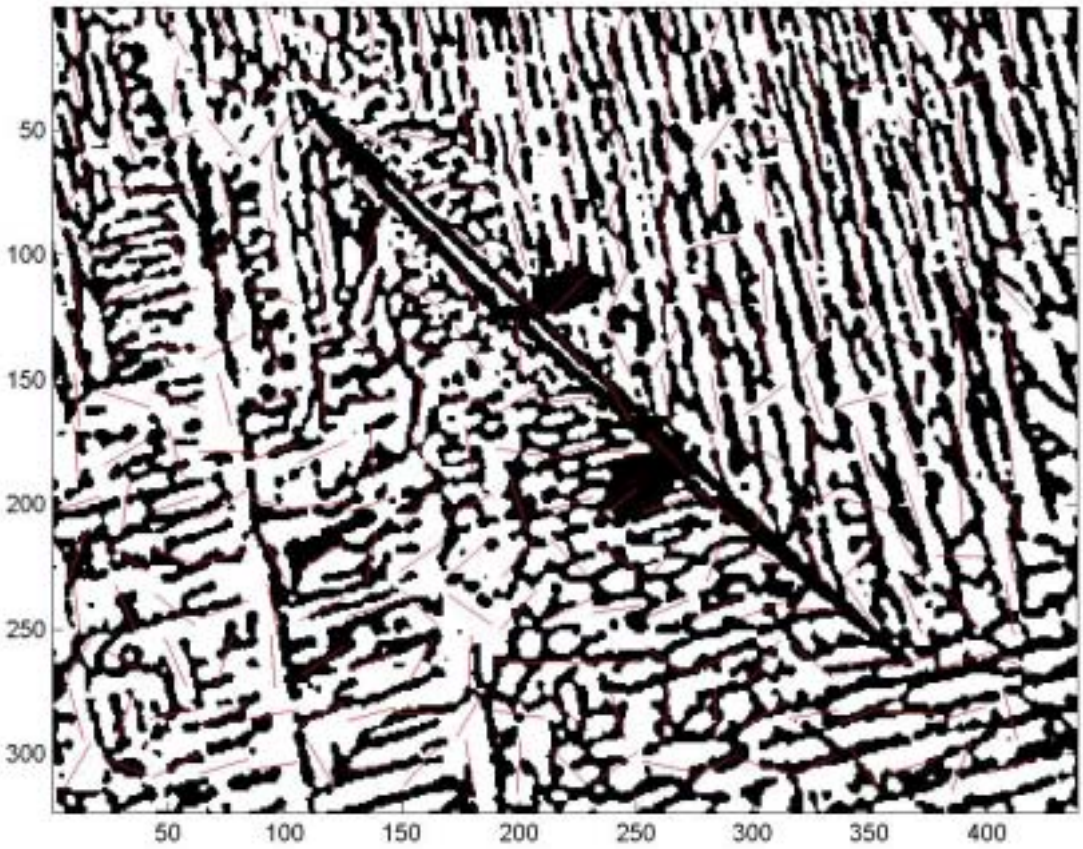

- Mask = 21, 6 classes:

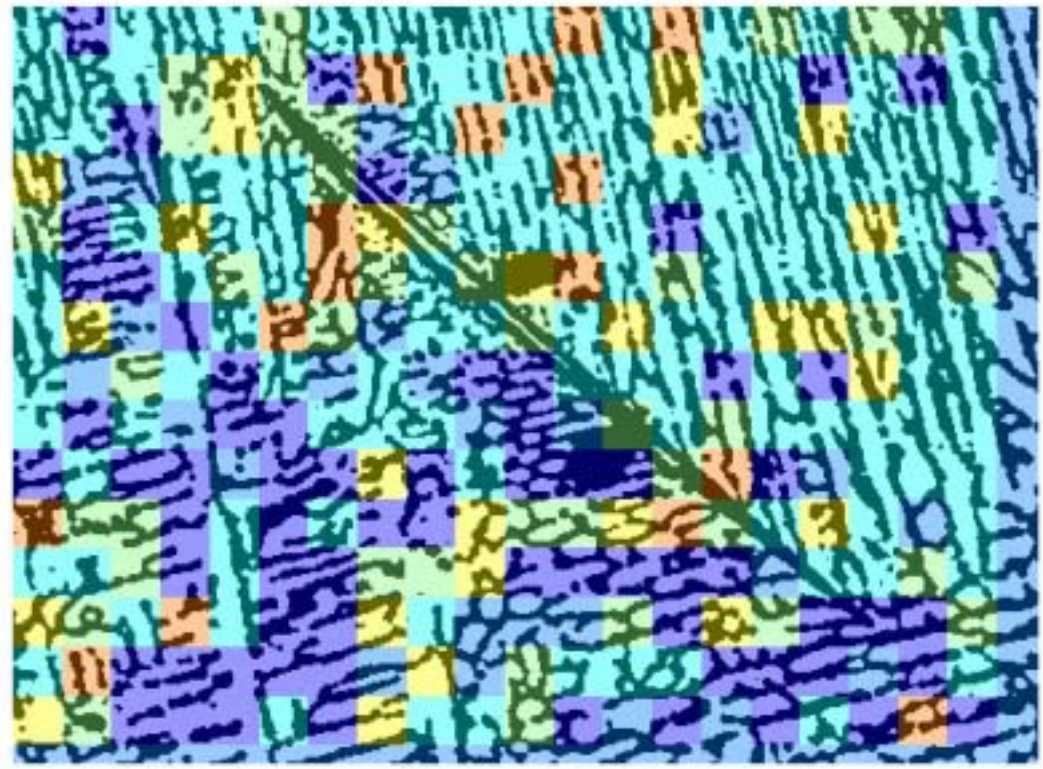

- Mask = 25, 130 seconds:

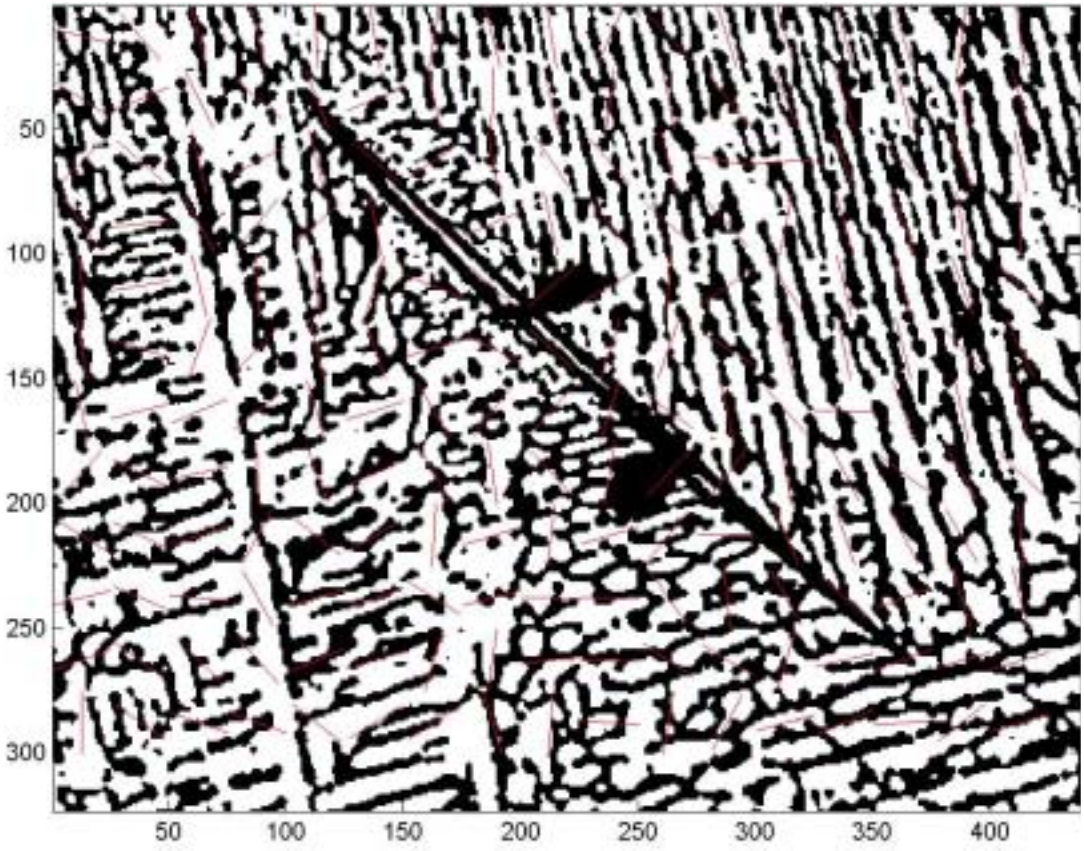

- Mask 25, 5 classes :

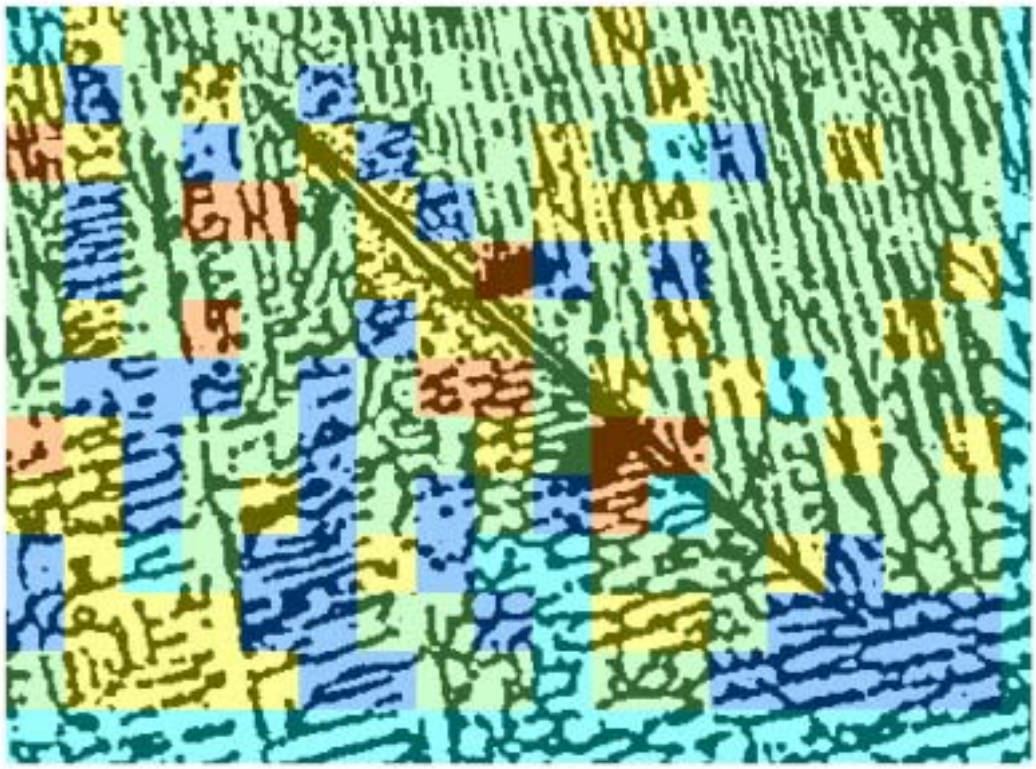

- Mask = 17, 5 classes:

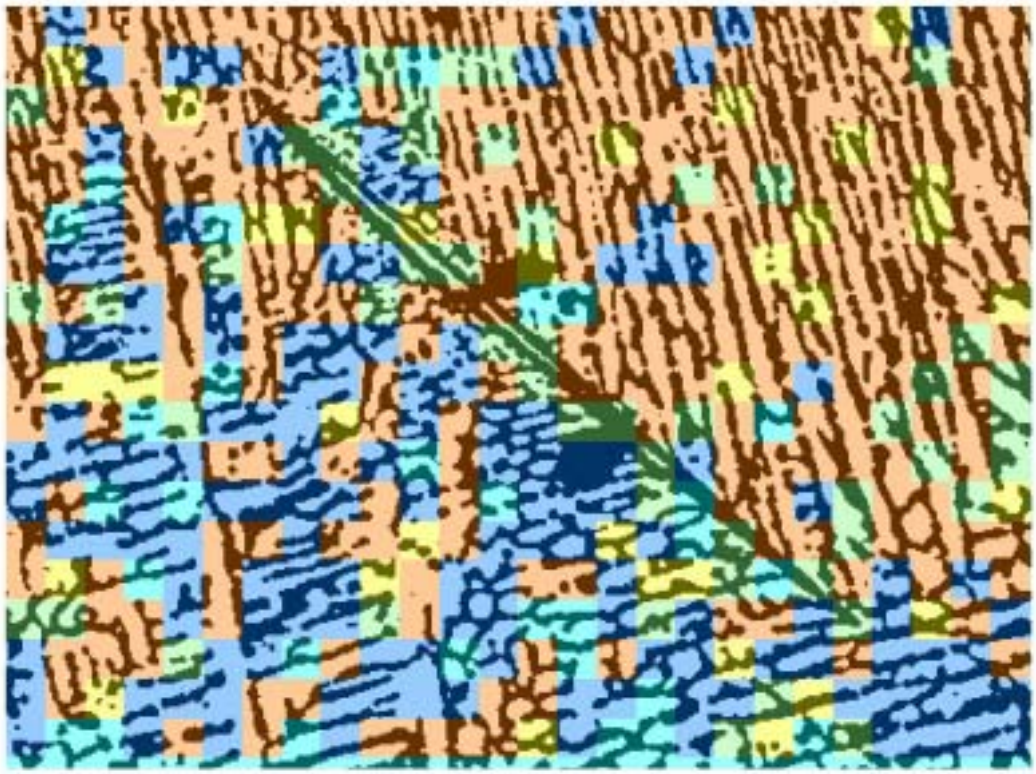

- Mask = 17, 4 classes:

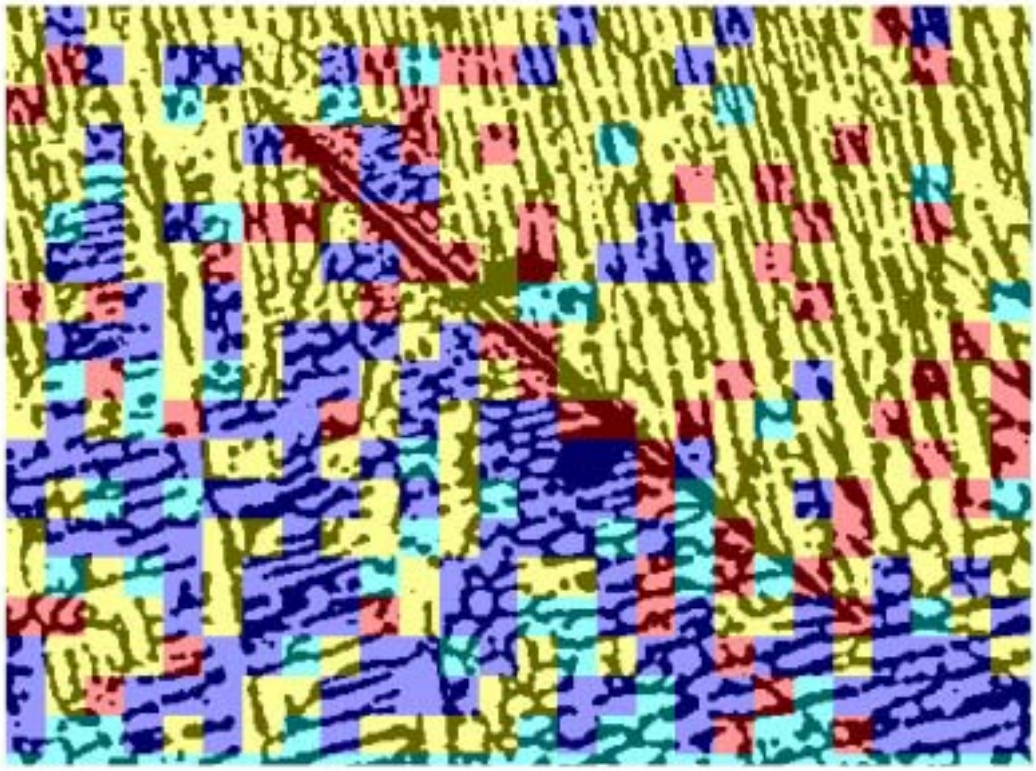

- Mask = 17, 3 classes:

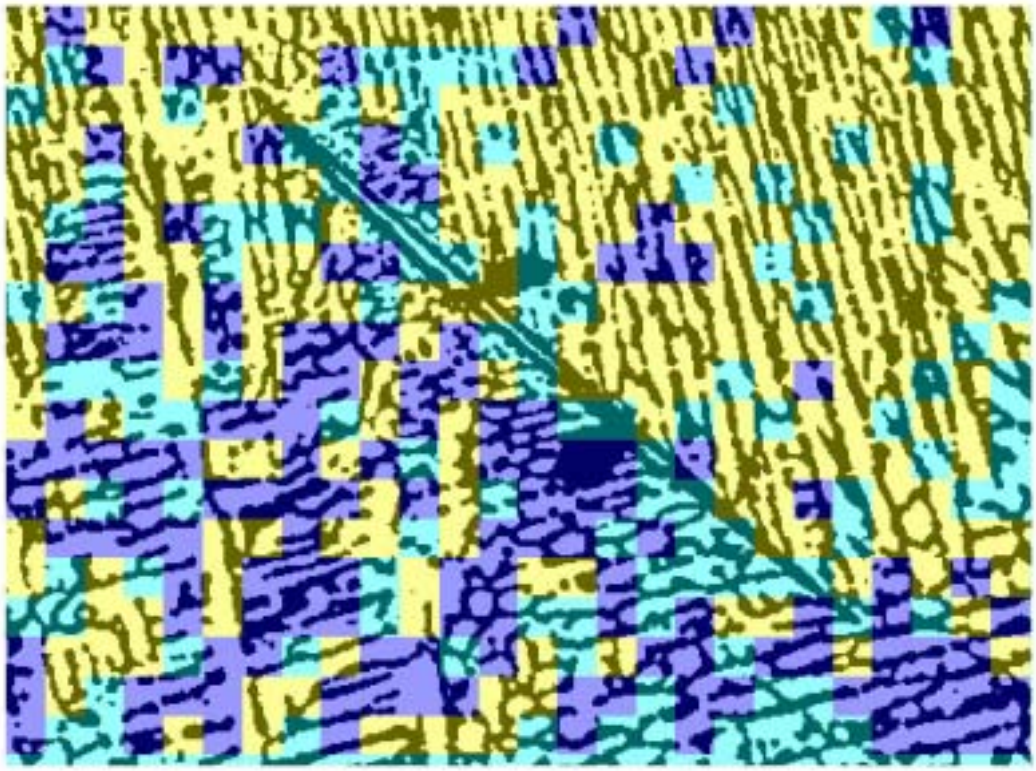

- Mask = 17, 2 classes:

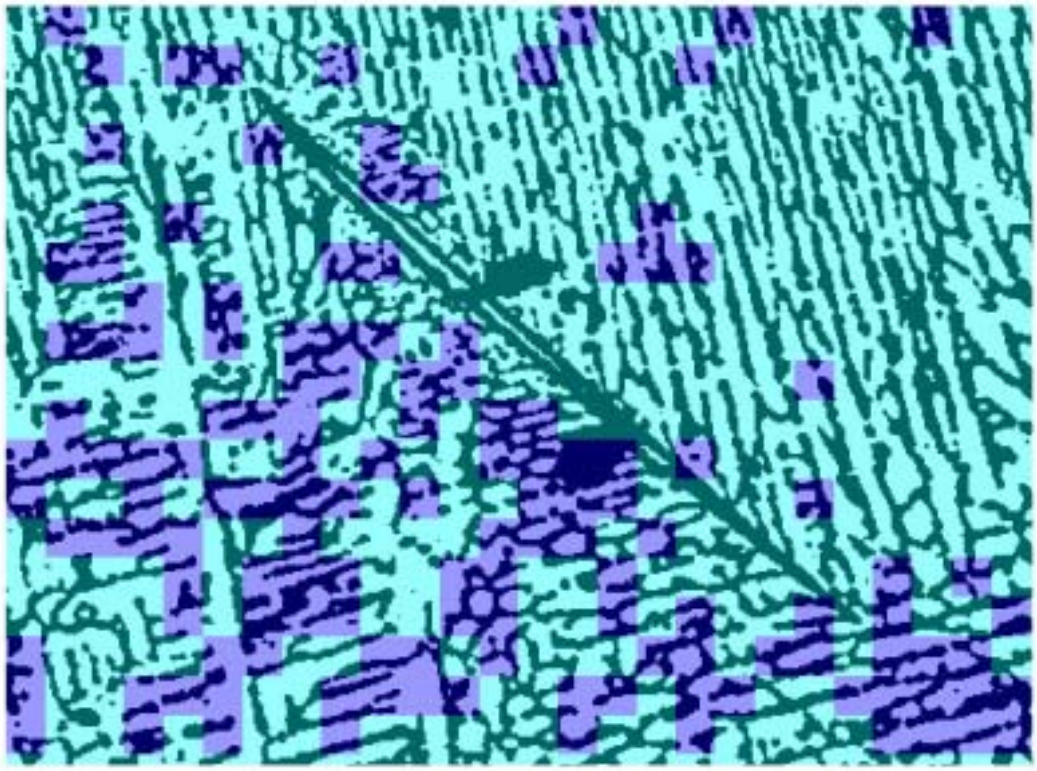

With one class, the image is obviously monochromatic.